This document was prepared in conjunction with work accomplished under Contract No. DE-AC09-96SR18500 with the U. S. Department of Energy.

DISCLAIMER

WSRC-TR-2005-00415

Evaluation of Enhanced VOC Removal with Soil Fracturing in the SRS Upland Unit

Brian D. Riha
Ken Dixon
W. Keith Hyde
SRNL

Larry Murdoch
Richard Hall
Clemson University

October 2005

Westinghouse Savannah River Company, LLC
Savannah River Site
Aiken, SC, 29808

SRNL
SAVANNAH RIVER NATIONAL LABORATORY

Prepared for the US Department of Energy under Contract DE-AC09-96SR18500

Contents

List of Attachments

List of Tables

List of Figures

Introduction

The Environmental Restoration Technology Section (ERTS) of the Savannah River National Laboratory (SRNL) conducted pilot scale testing to evaluate the effectiveness of using hydraulic fracturing as a means to improve soil vapor extraction (SVE) system performance. Laboratory and field research has shown that significant amounts of solvents can be entrapped in low permeability zones by capillary forces and removal by SVE can be severely limited due to low flow rates, mass transfer resistance of the hydrophobic compounds by trapped interparticle water, and diffusion resistance (Smith et al., 1996; Fisher et al., 1998; Yang et al., 1999; Oostrom et al., 2003).

Introducing sand-filled fractures into these tight zones improves the performance of SVE by 1) increasing the overall permeability of the formation and thereby increasing SVE flow rates, 2) shortening diffusion pathways, and 3) increasing air permeability by improving pore water removal. The synergistic effect of the fracture well completion methods, fracture and flow geometry, and pore water removal appears to increase the rate of solvent mass removal over that of increasing flow rate alone.

A field test was conducted where a conventional well in the SRS Upland Unit was tested before and after hydraulic fracturing. ERTS teamed with Clemson University through the South Carolina University and Education Foundation (SCUREF) program utilizing their expertise in fracturing and fracture modeling. The goals of the fracturing pilot testing were to evaluate the following:

- The effect of hydraulic fractures on the performance of a conventional well. This was the most reliable way to remove the effects of spatial variations in permeability and contaminant distribution on relative well performance. It also provided data on the option of improving the performance of existing wells using hydraulic fractures.

- The relative performance of a conventional SVE well and isolated hydraulic fractures. This was the most reliable indicator of the performance of hydraulic fractures that could be created in a full-scale implementation.

The SVE well, monitoring point arrays and four fracturing wells were installed and the well testing has been completed. Four fractures were successfully created the week of July 25, 2005. The fractures were created in an open area at the bottom of steel well casing by using a water jet to create a notch in the soil and then injecting a guar-sand slurry into the formation. The sand-filled fractures increase the effective air permeability of the subsurface formation and decrease diffusion path lengths for contaminant removal.

The primary metrics for evaluation were an increase in SVE flow rates in the zone of contamination and an increase in the zone of influence. Sufficient testing has been performed to show that fracturing in the Upland Unit accelerates SVE solvent remediation and fracturing can increase flow rates in the Upland Unit by at least one order of magnitude.

Background

Geology

The sediments within the A/M Area vadose zone consist of sand, sandy clay, clayey sand, and clay deposited from the middle to upper Eocene in shallow marine, lagoonal, or fluvial environments. These lithologies were deposited as layers or wedges and are commonly discontinuous due to depositional or post depositional processes (i.e., erosion).

Eddy and others (Eddy et al., 1991) identified four semi-confining/confining zones in this area. The upper three zones are semi-confining, clay rich or interbedded zones all above or within the M-Area aquifer zone. From the top down they are the “325 foot clay”, “300 foot clay”, and “270 ft clay” zones. The 325 foot clay and 300 foot clay are in the vadose zone and impact the flow of gases above the water table and recharge of air and water from the ground surface. The 270 foot clay is an interbedded zone that extends below the water table. The fourth, lowermost zone (not shown in Figure 1) is named the “200 foot clay” confining zone and corresponds to the “Green Clay” confining zone of the Steed Pond aquifer. The Green Clay separates the M-Area or water table aquifer from the Lost Lake aquifer zone. A schematic of the general geology along the old sewer line is provided in Figure 1.

The zone above and containing the “325 foot clay” is defined as the Upland Unit. This unit is fairly consistent across the SRS A/M Areas and is made up of a very low permeability, high porosity, high water content mix of sand, silt and clay and ranges from 10-50 ft thick at the SRS. The Upland Unit is approximately 35 ft thick at the pilot test site. Most facilities at the SRS were built on the Upland Unit, which has shown to entrap DNAPL for over 20-30 years (approximate time since releases ceased).

Solvent Behavior in the SRS Vadose Zone

Solvent releases at SRS were predominantly point sources (rubble pits, basins, drains, etc.) and line sources (multiple point sources) from process sewer lines. Observations from release sites at SRS indicate the solvents primarily moved downward as DNAPL with limited lateral spreading depending on the amount released and heterogeneity in the subsurface. At smaller release sites, the solvents remained in the Upland Unit with downward migration toward the water table controlled by gas diffusion. VOC removal from the fine-grained zones is assumed to be predominately diffusion limited. The conceptual model for solvent behavior in the SRS M-Area vadose zone is provided in Figure 2. This figure shows the cone penetrometer test (CPT) friction ratio log where higher numbers indicate finer-grained soils, high soil concentrations in the Upland Unit and decreasing soil gas concentrations in the Central Sandy Zone suggesting solvent movement could be primarily driven by gas diffusion. Mitigation of the solvent contamination in the Upland Unit is key for protection of groundwater.

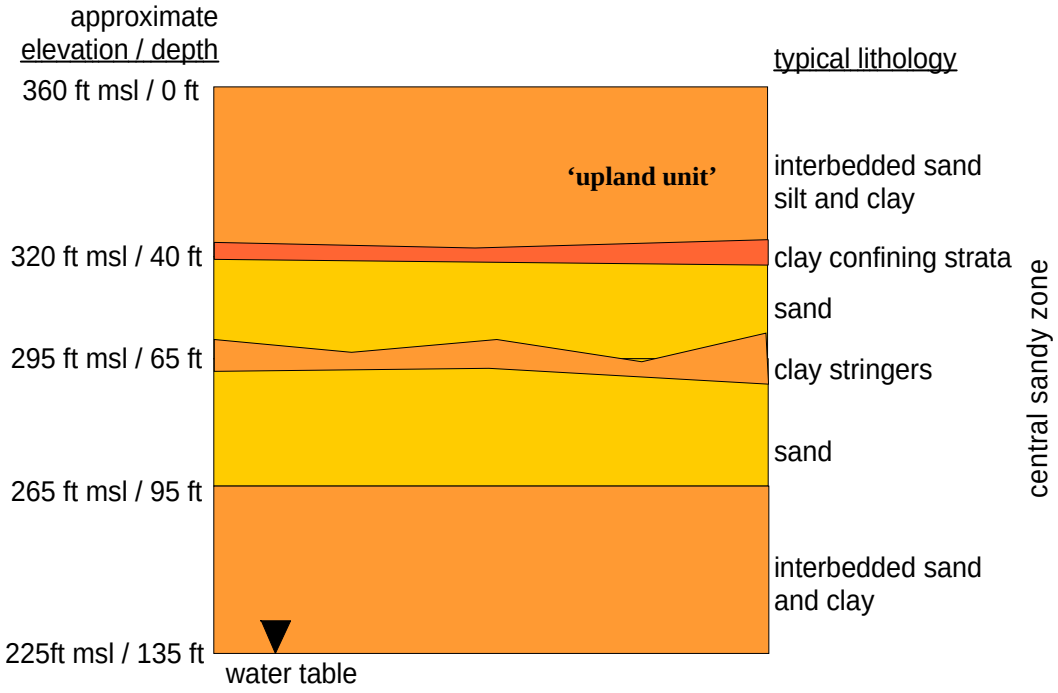

Figure 1 – General Stratigraphy at the SRS M-Area

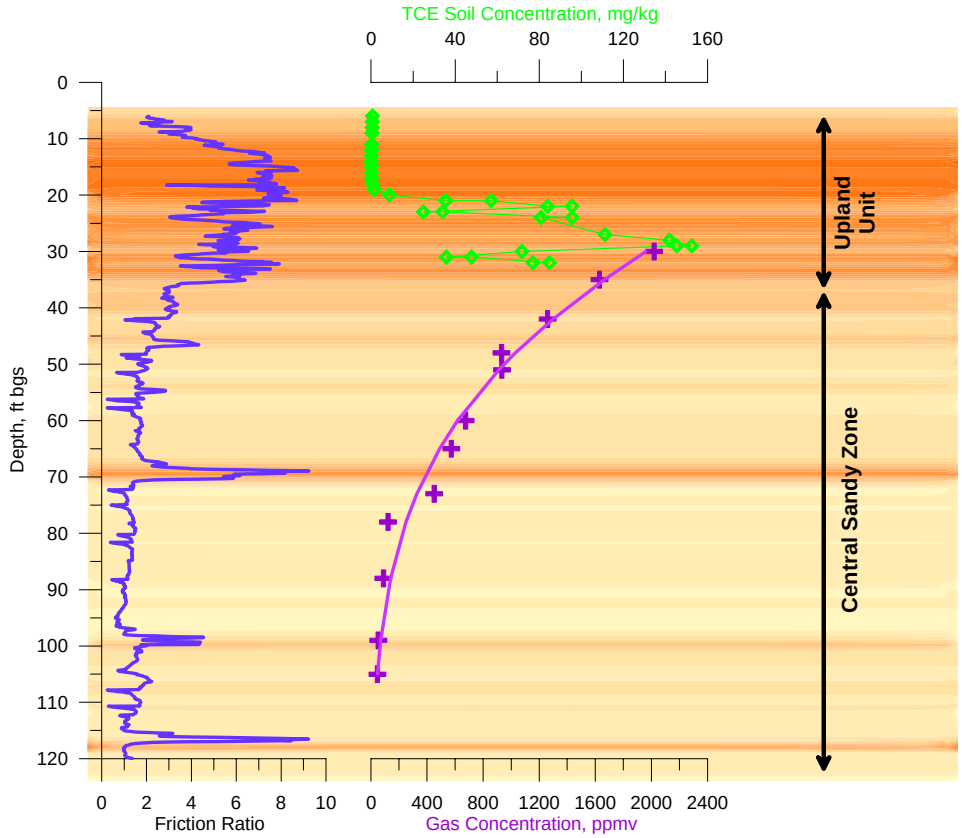

Figure 2 – Conceptual Model of Solvent Behavior in the M-Area Vadose Zone

Installation and Monitoring

Summary of Well and Boring Installations

One standard SVE well, four fracture wells, and twelve soil borings were completed to conduct the pilot study. The soil borings were installed for soil collection for VOC analysis and fracture identification. The general site layout is provided in Figure 3, measured distances are provided in Figure 4, and the boring method and brief installation details are summarized in Table 1.

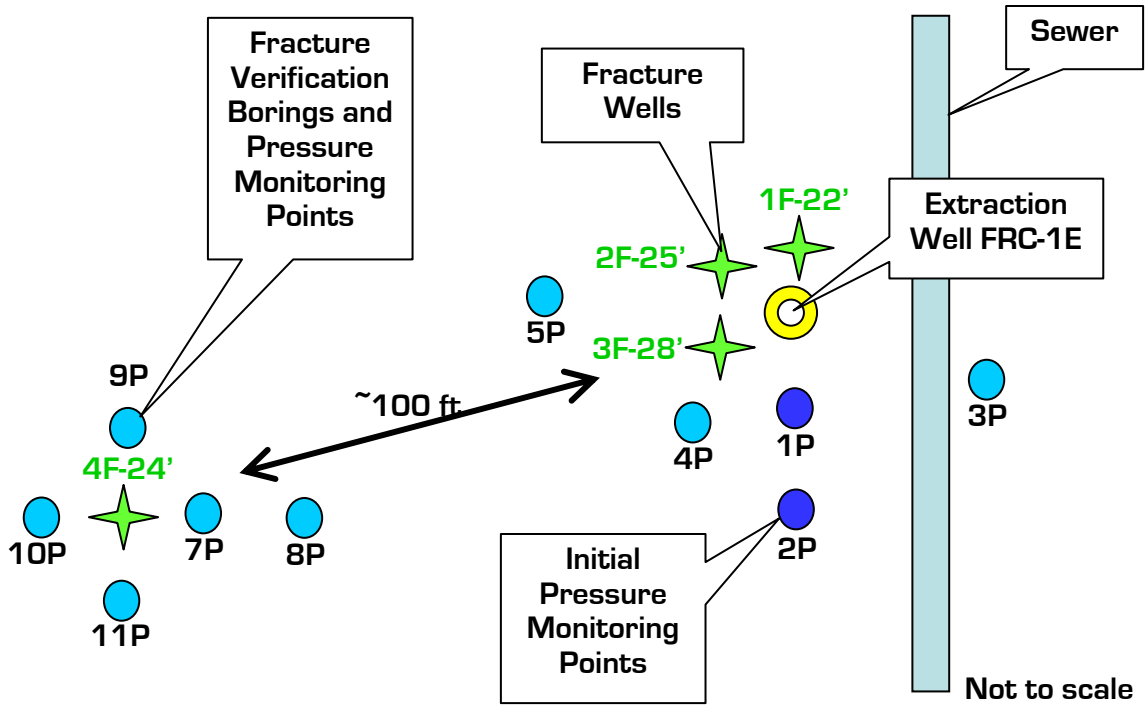

Figure 3 – General Pilot Test Site Layout

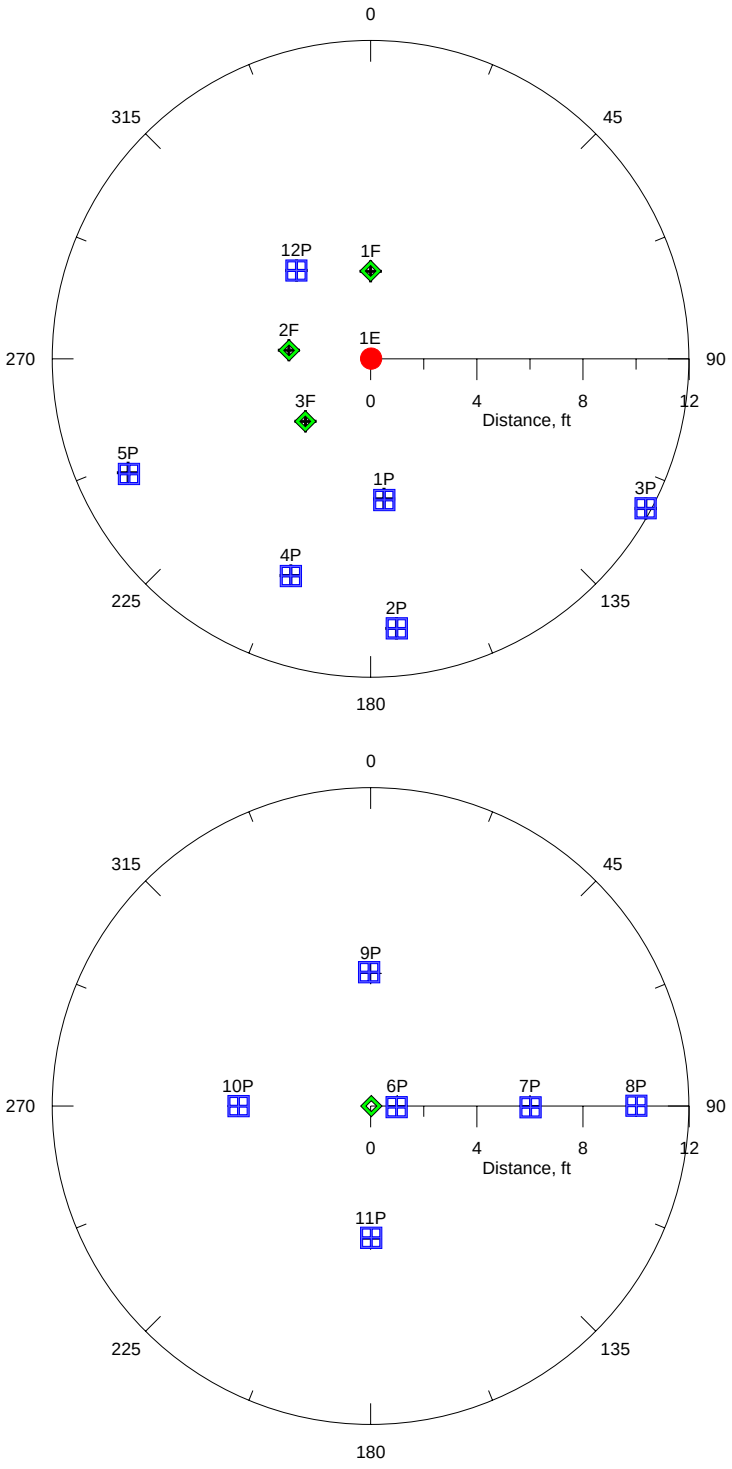

Figure 4 – Layout of Wells and Monitoring Points

Table 1 – Summary of Well and Monitoring Point Installations

Boring ID	Boring Method	Installation Details	Screen/Port Region, ft bgs	Depth Range for Soil Sample Collection, ft bgs
FRC-1E	Macro-core for soil samples. Hollow Stem Auger for well installation.	4 inch diameter stainless steel wire wrap screen	Screen 20-30 ft, 5 ft sump to 35 ft	6-32 VOC analysis
FRC-1P	CPT Wireline for soil samples	Flexible liner with sintered metal ports filled with sand	10, 15, 20, 22.5, 25, 27.5, 30	10-30 VOC analysis
FRC-2P	CPT Wireline for soil samples	Flexible liner with sintered metal ports filled with sand	15, 20, 25. 30	18-30 VOC analysis
FRC-3P	CPT Wireline for soil samples	Flexible liner with sintered metal ports filled with grout	18.5, 23.5, 28.5	13-30 VOC analysis
FRC-4P	CPT Wireline for soil samples	Single micro screen	30-31	13-29 VOC analysis
FRC-5P	CPT Wireline for soil samples	Flexible liner with sintered metal ports filled with grout	17.8, 22.8, 27.8	20-28 VOC analysis
FRC-6P	CPT Wireline for soil samples	no installation		20-29 VOC analysis
FRC-7P	CPT Wireline for soil samples	Single micro screen	19-22	16-25 VOC analysis
FRC-8P	CPT Wireline for soil samples	Single micro screen	17.5-21	12-21 Fracture ID only
FRC-9P	CPT Wireline for soil samples	Single micro screen	21.5-24.5	12-261 Fracture ID only
FRC-10P	CPT Wireline for soil samples	Flexible liner with sintered metal ports filled with grout	21, 23.5, 26, 28.5, 31	12-26 Fracture ID only
FRC-11P	CPT Wireline for soil samples	Single micro screen	20.8-25.8	12-26 Fracture ID only
FRC-12P	Hand auger	Single micro screen	26.6-28.2	none
FRC-1F	Direct push	2 inch diameter black steel pipe with sacrificial tip	22	none
FRC-2F	Direct push	2 inch diameter black steel pipe with sacrificial tip	25	none
FRC-3F	Direct push	2 inch diameter black steel pipe with sacrificial tip	28	none
FRC-4F	Direct push	2 inch diameter black steel pipe with sacrificial tip	24	none

Fracturing Methods and Results

Four fracturing wells were installed using hollow stem augering and direct push/hammering. These fracturing wells were constructed with two–inch nominal steel pipe with a sacrificial tip at the bottom. The sacrificial tip was pushed down 4-6 inches to expose the formation for fracturing. The SRS was issued Underground Injection Control (UIC) Permit 826 by the South Carolina Department of Health and Environmental Control (SCDHEC) to perform this pilot study.

The hydraulic fractures were created in a manner similar to that outlined in the document “Hydraulic Fracturing Technology, Technology Evaluation Report” (USEPA, 1993). Following this method, a radial notch was cut into the vadose zone sediments at the end of the fracture casing using a high pressure jetting tool referred to as a lance (Figure 5). This notch was used to initiate a hydraulic fracture. After the sediments were notched, a slurry of cross-linked guar gum gel and sand was injected at a constant flow rate into the 2-inch well using a progressive cavity pump. Injection was accomplished using a specialized mixer and pump (Figure 6). The purpose of the guar gum was to create a gel capable of suspending high concentrations of sand (Figure 7). An enzyme was added to the slurry to break down the gel several hours after injection. Once injection ceases, the resulting fracture starts to close as the gel seeps into the formation. The fracture is then held open by the sand that is left behind by the gel.

Figure 5 – Notching Well Prior to Hydraulic Fracturing

Figure 6 – Well Head and Fracturing Rig during Test

Figure 7 – Samples of slurry taken at different times during injection. Sand has settled to the bottom of the samples after gel break.

Three fractures (FRC-1F to 3F) were created at different depths from a tight cluster of wells with the intention of intersecting the gravel-packed interval of the extraction well. One fracture (FRC-4F) was created in a clean area roughly 100 ft (30 m) from the other three. FRC-4F was created first. A total of 1,350 lbs of sand was injected. The upper fracture in the cluster, FRC-1F, was created next at a depth of 22 ft. Slurry vented from a previously unrecognized open boring a few minutes after the start of injection FRC-1F. The open boring was revealed with a shovel and it was found to be open to a depth of 22 ft; the depth of the fracture initiation (Figure 8). The boring was sealed with cement grout and the FRC-1F was created the following morning. The other fractures were created in order of increasing depth, FRC-2F and 3F.

Figure 8 – Unrecognized open boring intersected by hydraulic fracture 1F.

The injection pressure measured at the well head increased abruptly to approximately 125 psi at the start of injection and then decreased as the fracture started to propagate (Figure 9). Pressure fluctuated during the first few minutes as the sand content in the gel was increased from small values up to the target load for the fracture. The pressure was typically in the range of 50 psi to 100 psi when the full load of sand in the slurry was being injected.

Two general styles of pressure logs were observed after the target sand concentrations were achieved. Injection pressure increased with time during 3F and 4F, and it was variable but roughly constant during 1F and 2F (Figure 9).

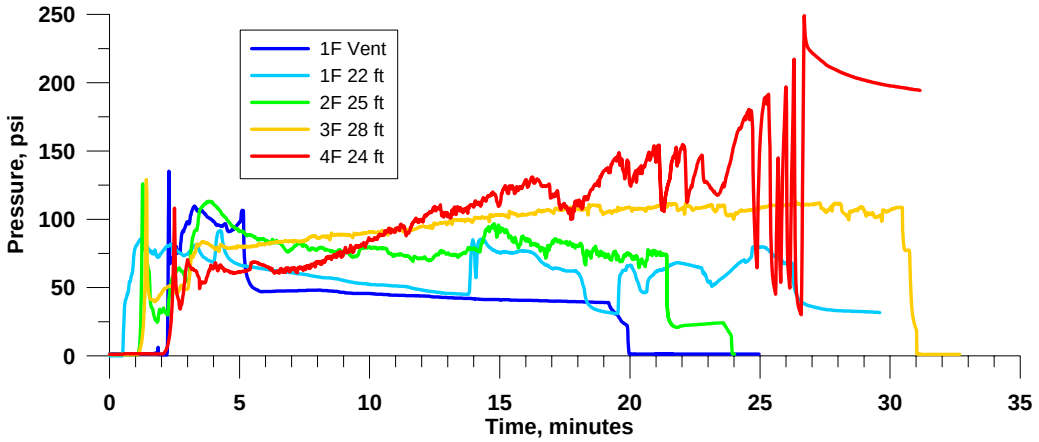

Figure 9 – Fracturing Pressure Logs

Injection pressure signals reflect interactions between the fracture and the enveloping formation, as well as engineering effects related to slurry properties, injection rates, and related processes. The initial injection pressure is relatively high because of the energy required to start propagation. Once the fracture has started to grow, the fluid pressure must separate the walls of the fracture, provide energy to break the formation, and overcome the viscous resistance as the slurry moves through the injection equipment and the fracture itself.

The pressure required to separate the fracture walls is essentially equal to the effective vertical stress $(\gamma_{formation} - \gamma_{slurry})d$, where γ is the unit weight and d is depth. Assuming the specific gravity of the soil solids is 2.65, and a moisture content of 0.15, $\gamma_{formation}$ = 120 pcf (lb/ft^3). The typical sand loading in the fractures is 10 lbs sand/gal gel, which gives γ_{slurry} = 100 pcf. So, the fluid pressure required at the well head is approximately 0.14 psi/ft depth. This gives 3 to 4 psi of wellhead pressure required to lift the overburden. The pressure at the depth of the fracture would be greater; approximately 0.83 psi/ft depth. This will be a small contribution to the observed injection pressures.

The fluid pressure required to break the formation progressively decreases as the fracture lengthens. This is the expected pressure response under ideal conditions. During the field tests, the pressure remained roughly constant (although variable) during 1F and 2F, and it increased with time during 3F and 4F.

Fluid pressure required to overcome viscous effects will be affected by changes in the fracture length or aperture, or by changes in the rheology (flow properties) of the injection fluid. The pressure will increase as the fracture lengthens or thins, but it can decrease if the fracture thickens. The slurry injected to create fractures during this test behaved as a shear-thinning power law fluid. The effective viscosity of the fluid will be a strong function of the ratio between sand and gel in the fluid. This ratio increases during and following injection as the liquid gel leaks out of the fracture. As a result, the effective viscosity of the injectate probably increases during injection, and this effect may be enhanced when the fracture cuts through relatively high permeability formations.

The increase of injection pressure during propagation of 3F and 4F, and the variations in the pressure of 2F are interpreted to be effects of changes in fluid rheology during injection. This occurs as the liquid phase separates and markedly increases the effective viscosity of the injection fluid. This process can essentially arrest slurry migration locally within the fracture. A similar process was inferred to occur in hydraulic fractures excavated and mapped by Jim Richardson near Clemson, and by other investigators in Cincinnati, Ohio. This process also occurs during hydraulic fracturing operations conducted by the oil industry, where it is called a “screen out”.

Table 2 provides the goal and the actual amount of sand injected in each fracture. The #1 filter sand ranges from 0.425 to 1.180 mm with a median grain diameter (D_{50}) of 0.70 mm. The #2 filter sand ranges from 0.600 to 2.000 mm with a median grain diameter (D_{50}) of 1.20 mm. The amount of water injected in each fracture is approximated based on 1 gallon of water for every 10 lbs of sand. A summary description of each plot in Figure 9 is provided in Table 3. These descriptions indicate the actual injection time in the SRS Upland Unit will require 30 minutes to reach the desired sand loading and that fractures propagate well in virgin soils in the Upland Unit.

Table 2 – Fracture Well Depth and Amount of Sand Injected

		Sand, lbs				Water, gallons (approximate)
ID	Depth, ft	Goal	Injected	#1	#2	
FRC-1F	22	1500	1000	1000	0	100
FRC-2F	25	2000	2000	1200	800	200
FRC-3F	28	2500	2500	1000	1500	250
FRC-4F	24	1500	1350	1350	0	135

Table 3 – Summary of Fracture Injections

Well ID	Depth, ft	Discussion
FRC-1F Vent	22	This fracture vented to the surface through an old borehole at approximately 5.5 minutes. This old borehole was sealed with grout.
FRC-1F	22	This fracture propagated but eventually vented to the surface about 7 ft northeast of the fracture well.
FRC-2F	25	Perfect fracture.
FRC-3F	28	Perfect fracture. This fracture was the largest sand-filled fracture created by the FRx, Inc in the past few years.
FRC-4F	24	Variations in pressure starting at 20 minutes possibly indicating screen out. Large variations in pressure at 25 minutes indicates sand bridging (blockage) in the hose, well, and/or fracture.

Fracture Geometry

Fracture depths and to some degree, areal extension were determined by soil core sampling. The three fractures around the SVE well FRC-1E were not found with core sampling. The surface and underground infrastructure did not allow sampling near the fracture origination points and detecting them away from the initiation points was not successful. Three CPT borings and one hand auger boring were attempted. The north side of the fracture site was inaccessible due to a steam line.

The fracture was identified in all 6 borings around the test fracture FRC-4F. The fracture was created at a depth of 24 ft, and it was discovered in cores at depths between 20 and 26 ft. The cores were obtained at distances from 1 ft to 10 ft from the injection well (Table 4). Pictures of the visually identified sand fractures from the soil cores are provided in Figure 10. These data were compiled to estimate the form of FRC-4F. The fracture is interpreted to be gently dipping to the west, with a maximum dip of approximately 25^{o}.

Table 4 – Location and Depth of Fracture FRC-4F

Boring ID	Distance from Fracture Point, ft	Direction	Fracture depth, ft
6P	1	east	24.0
7P	6	east	21.7
8P	10	east	20.0
9P	5	north	24.3
10P	5	west	26.0
11P	5	south	23.7

Figure 10 – Physically Observed Sand from Fractures during Coring

An average description of the fracture is provided in Table 5. Cross sections of the test hydraulic fracture FRC-4F facing East and North are provided in Figure 11. The fracture was identified in core samples (open circles) and interpolated in between. Extrapolation beyond the extent of the core samples is approximate and based on experience with forms of other fractures.

Table 5 – Fracture FRC-4F Description

Metric	Result
Average thickness	0.01 m (0.4 inches)
Average radius	4.5 m (15 ft)
Average depth	7.4 m (24.3 ft)
Average orientation	strike NS dip 25° W

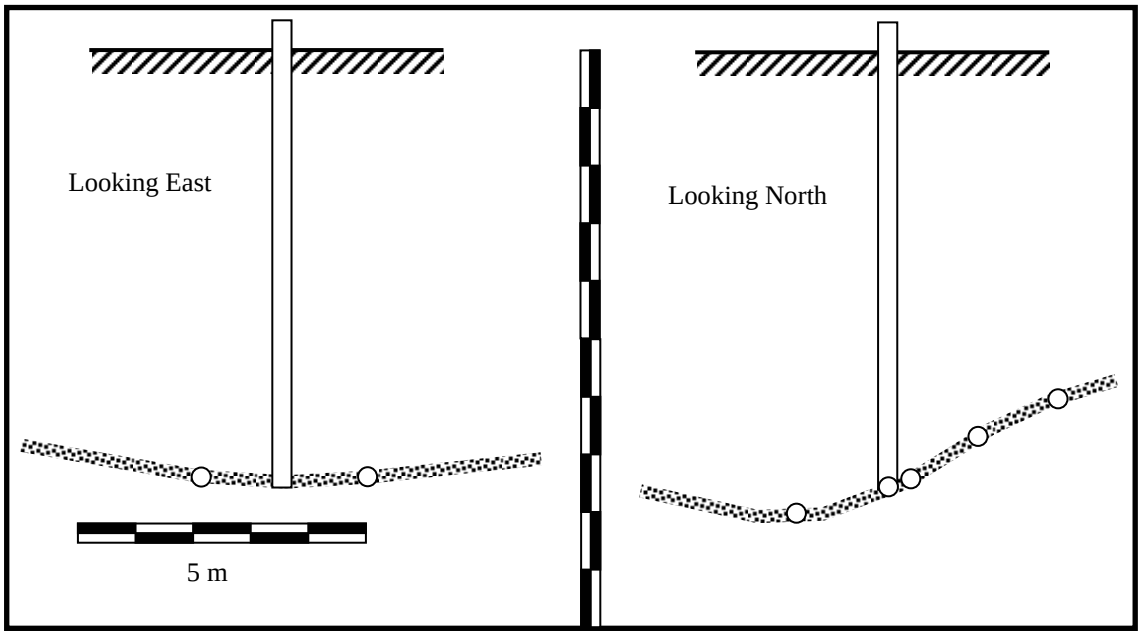

Figure 11 – Measured and Interpreted Fracture FRC-4F Cross-Sections

The thickness of sand in the cores from FRC-4F ranged from 1.5 to 2.5 cm (0.6 to 1 inch). This is thicker than expected based on analyses using expected parameter values for the area. The anomalous thickness could be a result of the screen out process discussed previously. The effects of screen out on fracture form are not included in available models, so it is approximated by increasing fracture toughness (both effects resist propagation and cause the predicted driving pressure to increase). Increasing the toughness will increase the injection pressure and thicken the fracture. As a result, the screen out process explains both the pressure log and the anomalously thick fracture.

The radial extent of the fracture is greater than 5 ft in all directions and greater than 10 ft in one direction (Table 4); however, the entire radial extent could not be established from field data because of insufficient sample locations to bound the maximum extent. The radial extent was estimated by assuming 1 cm (0.4 inch) as the average thickness of the fracture. This gives fracture an estimated fracture radius of 11.4 ft for 4F using the injected sand volume. The radii of the other fractures range from 9.8 ft to 15.5 ft, depending on the weight (volume) of sand injected and assuming the fractures are 1 cm thick and circular (Table 6).

Table 6 – Average radial extents of fractures estimated from injected sand weights. Assuming average fracture thickness is 1 cm.

	Sand weight injected	Average thickness assumed	Average radius estimated	
	lbs	inch	ft	m
FRC-1F	1000	0.4	9.8	3.0
FRC-2F	2000	0.4	13.8	4.2
FRC-3F	2500	0.4	15.5	4.7
FRC-4F	1350	0.4	11.4	3.5

SVE with Fractures Effectiveness Evaluation

Sediment Contaminant Distribution

Characterization efforts indicate residual VOC contamination remains in the fine-grained sediments in the pilot test area. The primary contaminant is TCE (trichloroethylene), with lesser amounts of PCE (perchloroethylene), and TCA (1,1,1-trichloroethane). Depth discrete TCE soil concentration profiles around the SVE well FRC-1E are provided in Figure 12. The yellow bars in the plot are the highest concentrations measured from all six soil borings. The maximum concentrations measured were 148 mg/kg TCE, 3.6 mg/kg PCE and 0.1 mg/kg TCA. Soil sampling and analysis methods and concentration results are provided in Attachment 1.

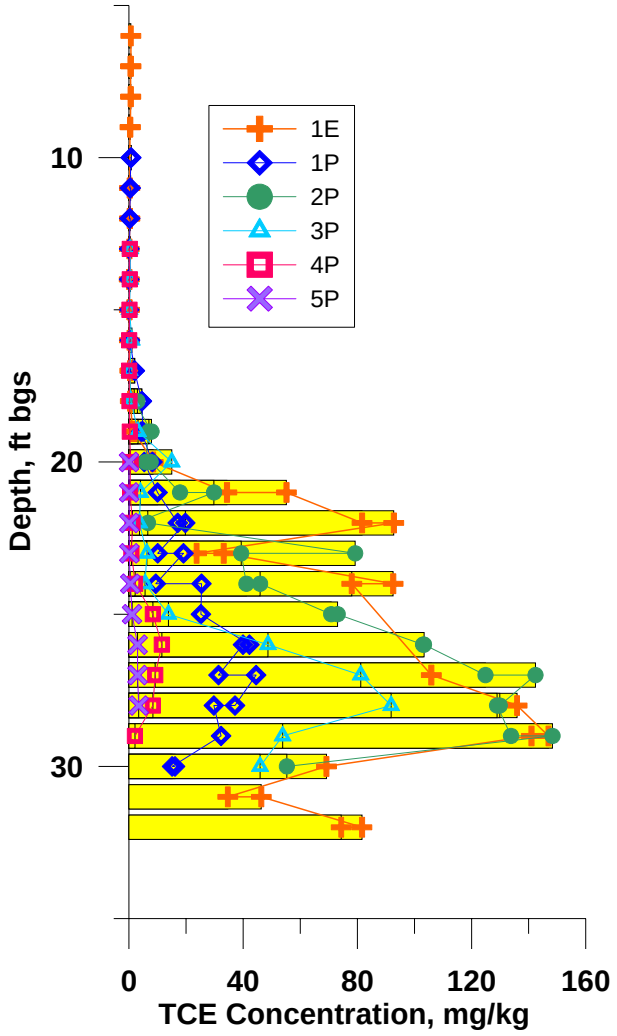

Figure 12 – TCE Soil Concentration Profiles

The TCE soil concentration data was imaged in three dimensions to aid in understanding the contaminant distribution in conjunction with the fractures. This image is provided in Figure 13 with a viewpoint from the southwest. The fractures are idealized at a 10 ft radius with horizontal propagation. Based on this image, the fractures should intersect the most contaminated regions in the system.

The contaminant concentration increases with depth to reach a maximum between 27 and 29 ft (Figure 12 and Figure 13). Interpretation of air pressure distributions during SVE testing suggests that there is a stratigraphic layer with a relatively low permeability between 24 ft and 28 ft. It appears that the maximum contaminant concentrations occur in this low permeability layer.

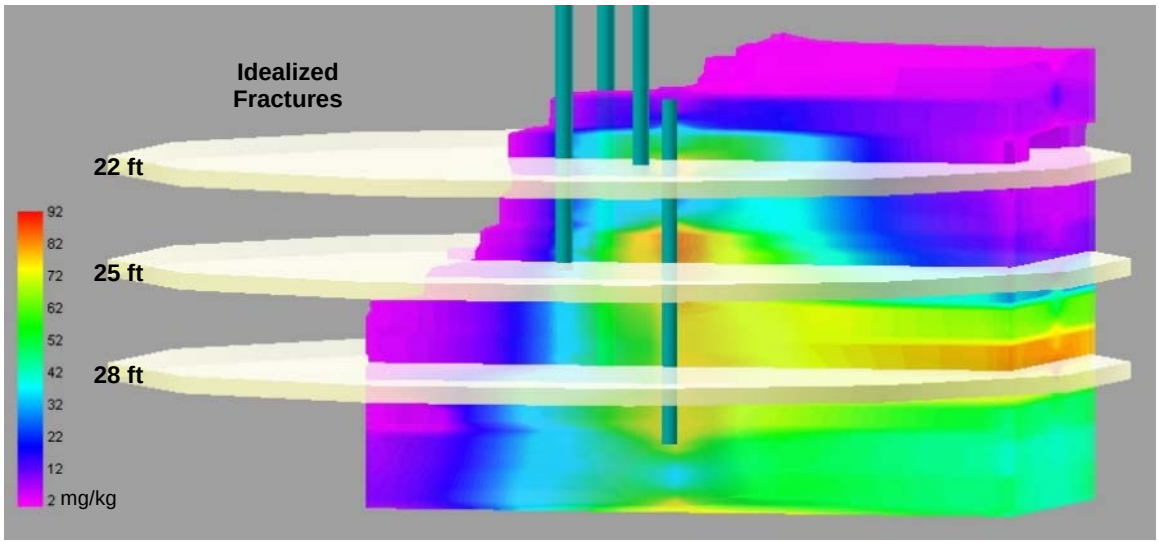

Figure 13 – 3D Image of TCE Soil Concentration with Approximate Fracture Locations

Comparison of SVE Flow and Zone of Influence

A portable, trailer-mounted vacuum unit was used for SVE testing purposes with power supplied by a portable diesel generator. The unit was connected to the extraction wellhead with 2 inch diameter flexible tubing and a PVC manifold. A photograph of the pilot test is provided in Figure 14. A pumping test was conducted on the extraction well prior to creating the fractures and flow, pressure, and composition of the produced gas were measured over time. Two pneumatic piezometers (FRC-1P and FRC-2P) were used to monitor vadose zone pressures during the SVE test. The test on the extraction well was used to establish the baseline flow rates and zone of influence (ZOI) based on pressure achievable with standard SVE well installations in the Upland Unit. The flow rate achieved was 2.7 scfm at 367 inches water (27 inches of Hg) vacuum for the 10 ft screened SVE well without fractures.

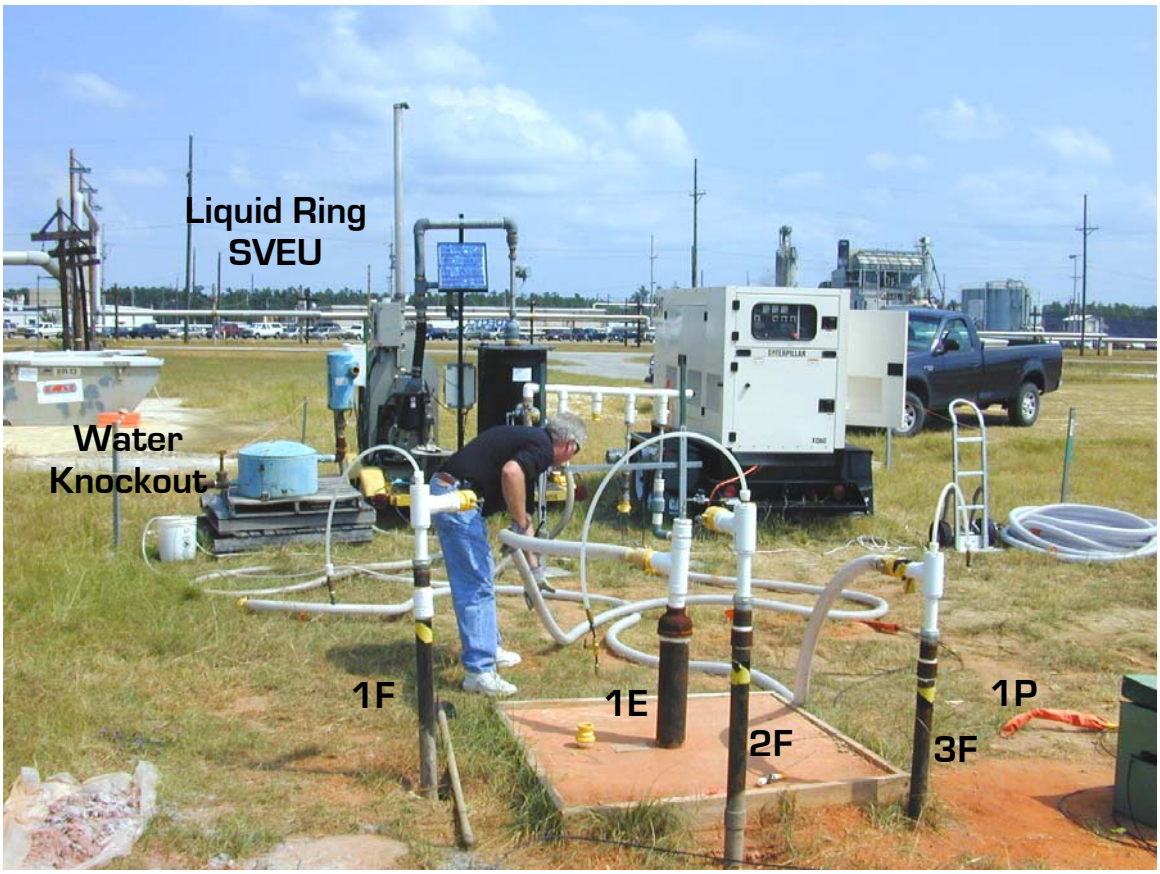

Figure 14 – Picture of the Pilot Test Site around FRC-1E

A second pumping test was conducted on the extraction well after the fractures were created. The pumping system was configured for dual phase recovery to remove residual water remaining in the fractures. Fracture casings were used as piezometers, along with the existing pneumatic piezometers. Pressure drawdown plots from depth discrete pressure monitoring points for SVE well FRC-1E are shown in Figure 15 and Figure 16 for pre and post fracturing, respectively. These plots indicate that the measured ZOI based on pressure increased after fracturing. The pressure exceeded the range of the pressure transducers at the deeper monitoring points and these were not plotted in Figure 16.

The drawdown data was imaged at steady-state conditions around the well FRC-1E assuming symmetry. The pre-fracture contour (Figure 17) shows limited ZOI with a well vacuum of 367 inches of water (27 inches Hg). This image implies the permeability increases slightly with depth. The monitoring point arrays FRC-1P and FRC-2P were used for this analysis.

The post-fracture contour (Figure 18) was imaged assuming horizontal fractures and a constant pressure in the fractures in addition to the monitoring point arrays.

This figure shows a significant increase (order of magnitude) in the measured ZOI at a lower SVE well vacuum of 230 inches of water (17 inches Hg).

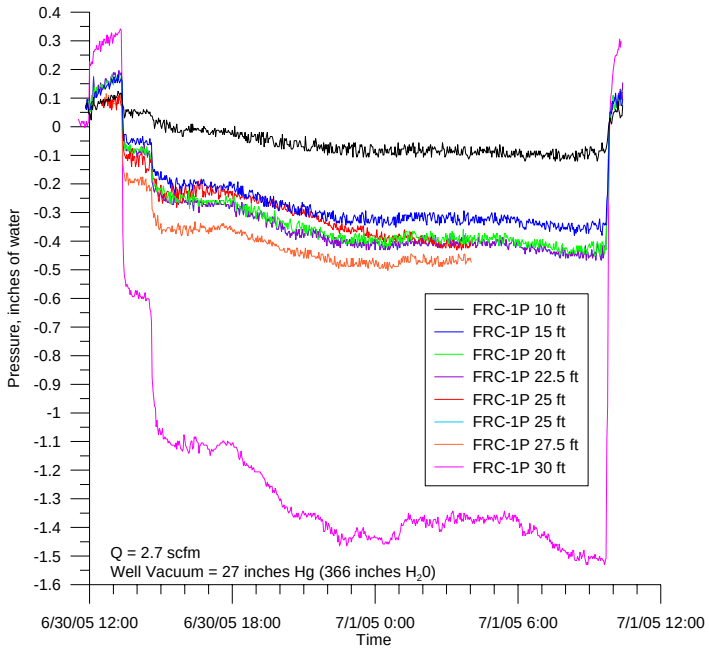

Figure 15 – Pre-Fracture ZOI from SVE Well FRC-1E

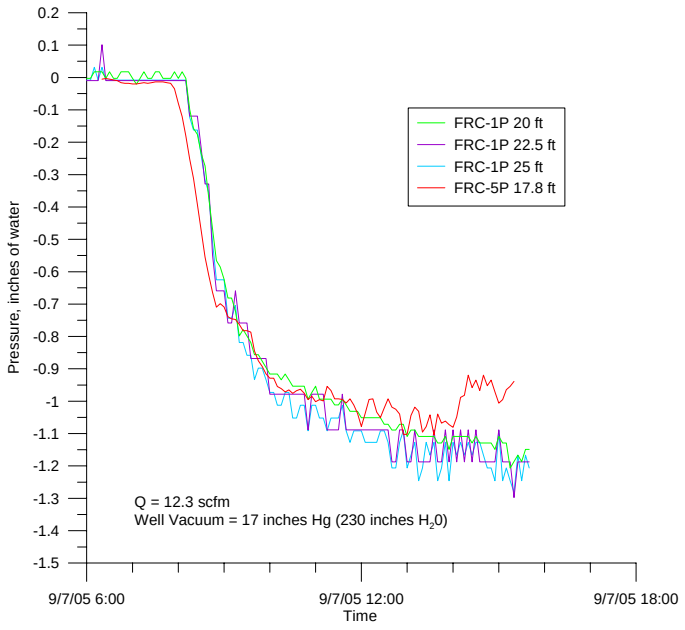

Figure 16 – Post-Fracture ZOI from SVE Well FRC-1E

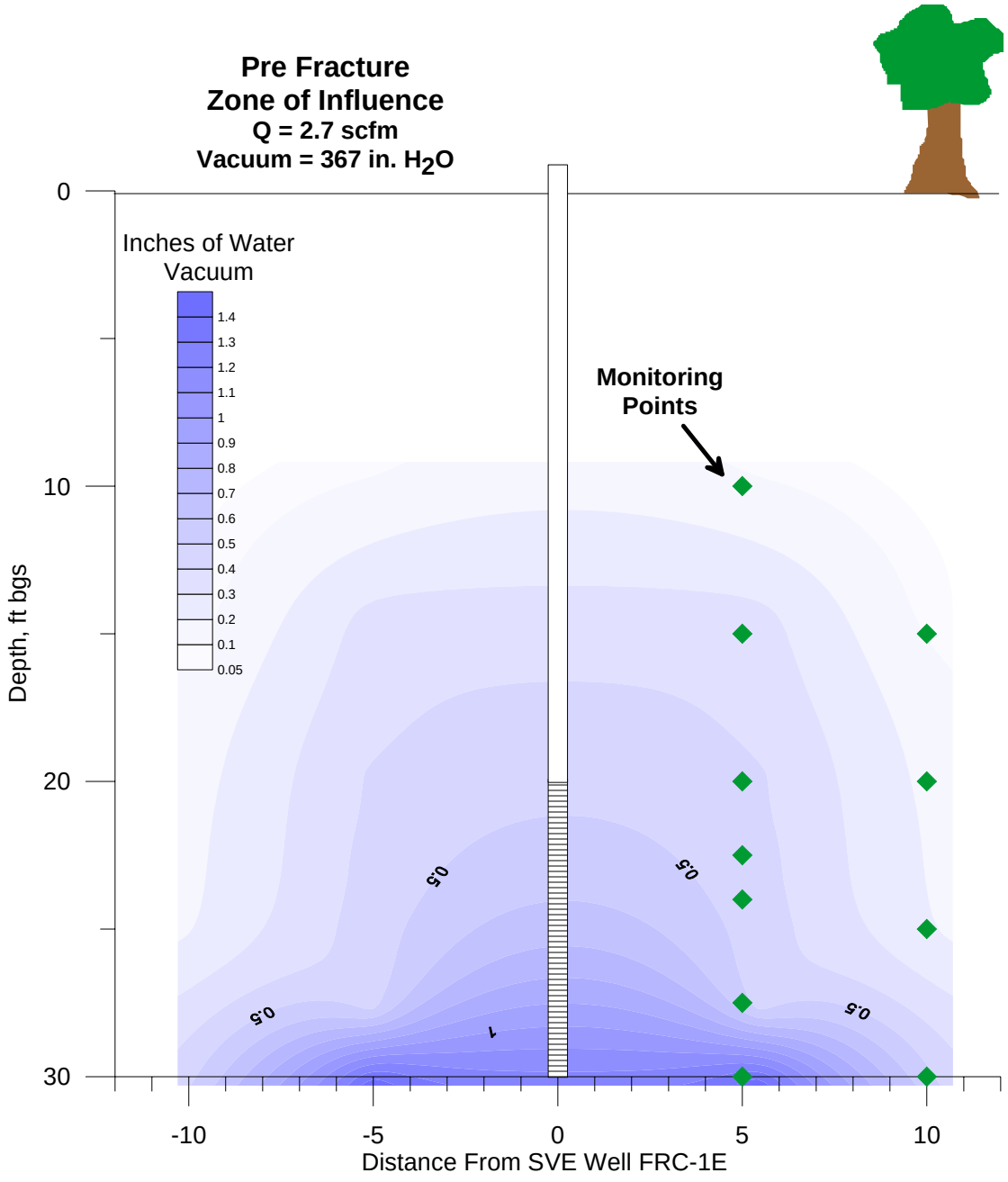

Figure 17 – Pre-Fracture ZOI Contour for FRC-1E

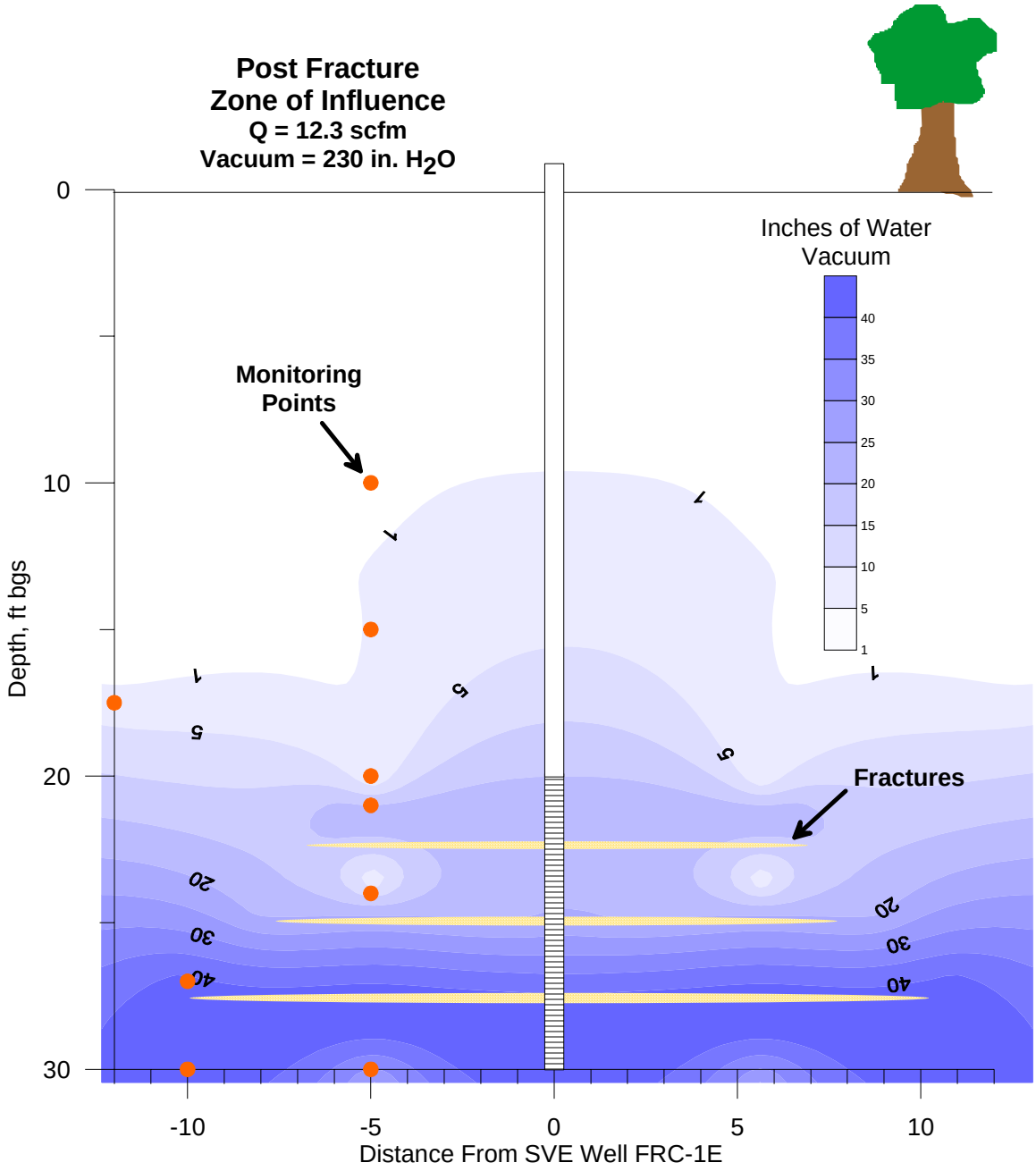

Figure 18 – Post-Fracture ZOI Contour for FRC-1E

Additional pumping tests were conducted using each fracture casing as an extraction well. The purpose of these tests was to evaluate the transmissivity of the hydraulic fractures in the vicinity of the conventional well. The vacuum applied and resulting flow rate from the SVE well and fracture wells after fracturing are provided in Table 7.

Table 7 – Vacuum and Flow Rates after Fracturing

Well ID	Applied Vacuum inches Hg	Flow Rate SCFM
FRC-1E	10	3.6
FRC-1E	25	10.3
FRC-1F	10	5.9
FRC-2F	10	2.0
FRC-3F	10	30
FRC-4F	10	30

It appears the fractures do not have very good connectivity with the original SVE well. If the fractures had intersected the well screen as hoped, the total flow should have been close to the total flow of the three fractures (3.6 scfm versus 37.9 scfm at 10 inches Hg). The fractures likely pinched off at the hollow stem auger well skin. Fracturing towards existing SVE wells in the SRS Upland Unit is not viable. Based on these results, by using the fracture wells as extraction wells, flow rates in the Upland Unit at the SRS can be increased by at least an order of magnitude.

Summary of Flow Modeling

This section provides a summary of results from numerical flow modeling conducted by Clemson University to assist in evaluating soil fractures on the enhancement of SVE in the SRS Upland Unit. Both homogeneous and heterogeneous modeling were conducted for this portion of the Upland Unit. The most significant finding was the existence of a low permeability 'well skin' around the conventional SVE well installed with hollow stem auger drilling. The full modeling report will be issued as a separate document.

Data from the gas pumping tests were used to estimate formation permeability and skin factors on the conventional well. This was done first using analytical solutions described by Bradner and Murdoch (2005). The analytical solutions were fit to the field data using a parameter estimation scheme. Those results served as the starting point for numerical analyses that attempted to fit the field data using T2VOC. Parameter estimation methods implemented by the software PEST were used to determine the average permeability, assuming homogeneous conditions. The numerical approach was then used to estimate permeability distribution in a layered system.

To improve the predictions of the field data, another analysis was conducted using a heterogeneous model that included four, flat lying layers of different permeability and a well skin with two different permeabilities. The two different skins were located according to the position of the formation layers relative to the well bore. This model provided the most realistic fit to the field data. The model material distributions and resulting fitted formation permeabilities are shown in

Figure 19. Correlations between observed and model fitted pressure distributions are shown in Figure 20.

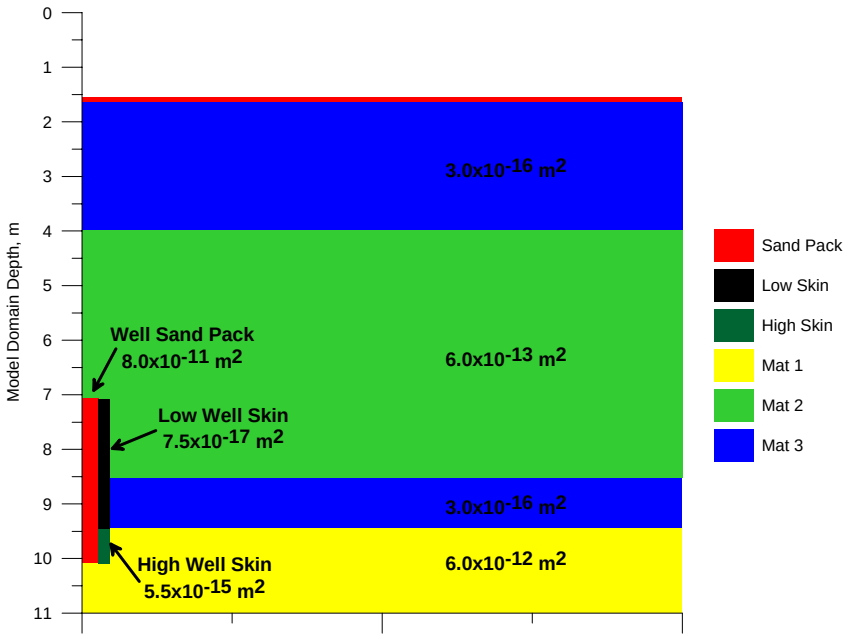

Figure 19 – Material Distribution and Fitted Permeabilities for the Two Skin Heterogeneous Model

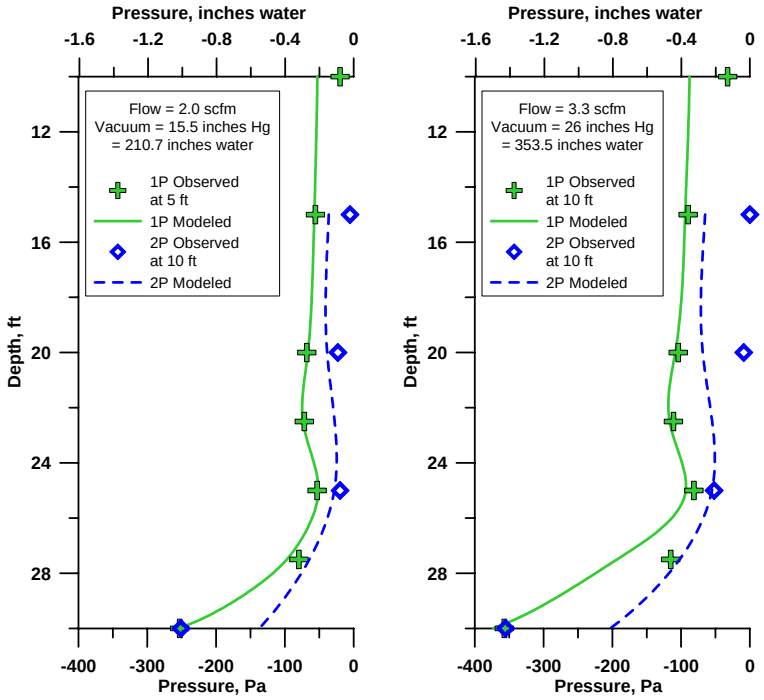

Figure 20 – Correlations between Observed and Modeled Pressure Distribution Prior to Fracturing: Two Skin Heterogeneous Model

Results of the modeling efforts consistently indicate the presence of a low permeability skin on the conventional SVE well. Similar results were reported by Bradner and Murdoch (2005) for SVE wells in saprolite near Clemson. The skin factors determined for this study are all significantly greater than those found by Bradner and Murdoch, however. For example, skin factors for wells created with an auger were roughly 25 in the study by Bradner and Murdoch, whereas they are roughly an order of magnitude greater at the conventional SVE well tested in the SRS Upland Unit.

Creating wells that are free from well skin using conventional drilling methods appears to be difficult, at least according to the results of Bradner and Murdoch. They used three different drilling methods, tried brushing the well bore, and took special care to block water from the well bores during completion. The effect of skin could be reduced using those methods, but the well performance was always significantly less than optimal as a result of the skin that remained. It is important to recognize, however, that this study was conducted in the Piedmont, and different results may occur in Coastal Plain sediments. Published descriptions of well skin on SVE wells other than those by Bradner and Murdoch are scarce.

Hydraulic fractures are known to improve well performance through two mechanisms. The permeable layer created by hydraulic fracturing changes the flow paths in the vicinity of a well, and this reduces head losses and improves well performance. This effect improves performance relative to a conventional well created in ideal conditions, and the extent of improvement depends largely on the ratio between the permeability of the formation and the permeability of the sand in the fracture. The other effect is that hydraulic fractures can cut the low permeability layer produced by the drilling process and otherwise recognized as skin.

As a result of these two effects, wells intersecting hydraulic fractures can perform better than conventional wells in part because of the geometric advantages of the hydraulic fracture, but also in part because conventional wells are damaged and their performance is degraded by skin.

One result of this understanding is that hydraulic fracturing can be viewed as a method of well completion, rather than a specialized technique done to improve the performance of an existing well. A consequence of this is that hydraulic fracturing may become a routine method for completing wells in some formations where skin is particularly problematic. This approach is common in the energy industry. Wells in many tight oil and gas reservoirs are fractured routinely as part of the well completion process.

Trends of flow rate predicted for the different hydraulic fractures resemble field observed trends. The flow rate is relatively high from the shallowest fracture, it diminishes in the middle fracture and is highest in the lowest fracture (Table 8).

Numerical values of the predicted flow rates are somewhat different than the observed values, but that is understandable in view of the simple way that the fractures were represented.

Table 8 – Flow Results: Field Measurements and Heterogeneous and Homogeneous Model Fits

Applied Vacuum	Extraction Well	Field Test Flow, scfm	Heterogenous Fit Flow, scfm	Homgeneous Fit Flow, scfm
10 inches Hg	FRC-1E	3.64	25.7	33.40
	FRC-1F	5.86	6.4	10.46
	FRC-2F	1.13	0.2	10.46
	FRC-3F	24.50	12.4	10.46
20 inches Hg	FRC-1E	10.96	42.0	56.50
	FRC-1F	9.40	10.3	18.32
	FRC-2F	1.34	0.3	18.32
	FRC-3F	32.00	21.0	18.32

The flow rate from the conventional well is predicted to be much greater than was actually observed. One objective of this project was to evaluate the viability of using a conventional well to produce air from hydraulic fractures, and this design was based on the expectation that the yield from the conventional well would be increased just as predicted in the analysis (Table 8). However, the observed flow rate from the conventional well was almost an order of magnitude less than predicted. Details of how hydraulic fractures interact with existing wells are not well known. It seems likely that the aperture of the fracture decreases in the vicinity of the conventional well, reducing the effectiveness of the hydraulic fractures. This finding is consistent with results from other sites.

The relatively low flow from the middle fracture (2F) was unexpected and it was difficult to explain this observation based on the field data alone. However, the modeling analysis confirms this behavior and provides an explanation. The yield from 2F was lower than the other two fractures because 2F was created in the bed whose conductivity was much lower than that of the other two fractures. On one hand, the yield from 2F was disappointing, but on the other hand, the results from the model suggest that this fracture is specifically targeting the lowest permeability layer. SVE using 2F could be focused on the lowest permeability layer. This is important because VOC contaminant concentrations are commonly greater in low permeability zones and are more difficult to remediate than overlying or underlying zones of greater permeability. Moreover, completing each fracture with its own well casing would allow individual zones to be targeted, which would be infeasible when using a conventional well screened across low and high permeability layers.

Estimated Mass Removal Effectiveness

Since SVE effectiveness is based on air flow through the contaminated zone, mass removal and the benefit of fracturing in the Upland Unit was initially compared based on flow rates alone. Based on the pre and post fracturing SVE testing, it is estimated that flow rates can be increased by at least an order of magnitude in the Upland Unit at the SRS.

It is postulated that soil concentrations will decline exponentially similar to the decline in off gas concentrations commonly observed during SVE at the SRS. Based on this assumption, soil concentrations can be estimated with the following time based decay equation:

$$C_t = C_0 e^{-kt_{days}}$$

where

C_t = concentration at time t (mg/kg)
C_0 = initial soil concentration (mg/kg)
k = decay constant (day^{-1})
t = time (day)

For calculation purposes, a 10 ft diameter by 10 ft high cylinder of soil is evaluated as a treatment zone. From the average dry density of soil in the Upland Unit of 104.3 lb/ft^3 (1.67 g/cm^3), this cylinder contains 148,628 kg of soil.

As an example, using contamination levels and cleanup goals for an area of the SRS M-Area, cleanup timeframes were compared for SVE with and without fractures in the Upland Unit. The calculations use the following assumptions:

- Fractures will increase flow rate by 1 order of magnitude
  - Compare flow rates at 1 and 10 scfm
- Flow is throughout the entire cylinder
- Maximum concentration is constant throughout cylinder
- Removal is exponential decay
- Soil concentrations and total mass
  - TCE at 400 mg/kg = 59,450,000 mg TCE in cylinder
  - PCE at 12,300 mg/kg = 1.828x10^9 mg PCE in cylinder
- Average SVE removal concentration
  - 100 ppmv (15.48 mg/ft^3) TCE
  - 1000 ppmv (195.30 mg/ft^3) PCE
- Decay constant (k) can be approximated by daily mass removal divided by the total mass in the system

These assumptions are based on the measured flow rates with and without fracturing, soil concentrations measured in the Upland Unit at the SRS M-Area,

and historical SVE behavior observed and measured at the SRS. The calculated results are summarized in Table 9. These results show that an increase of the flow rate by a factor of 10 increases the decay constant by a factor of 10.

Table 9 – Summary of Theoretical Mass Removal Rates with and without Fracturing

VOC	Average SVE Concentration	Soil Concentration/ Total mass in the Soil Cylinder	Flow without Fractures 1 scfm	Flow with Fractures 10 scfm
TCE	100 ppmv (15.48 mg/ft^3)	400 mg/kg 59,451,200 mg	22,291 mg/day k=0.0004/day	222,912 mg/day k=0.004/day
PCE	1000 ppmv (195.3 mg/ft^3)	12,300 mg/kg 1,828,126,131 mg	281,232 mg/day k=0.0002/day	2,812,320 mg/day k=0.002/day

For this example, two cleanup goals are used. The higher cleanup goal is the principal threat source material (PTSM) contaminant of concern (COC) and the lower goal is the contaminant migration (CM) COC. Since soil fracturing is deemed a semi-aggressive remediation technique, it is being evaluated to address the PTSM cleanup goals. Plots for TCE and PCE soil concentration decline for SVE with and without fracturing are provided in Figure 21 and Figure 22. The PTSM and CM cleanup levels along with the projected time for reaching the PTSM goal without fracturing are provided in the figures. From this analysis, the time for remediation to reach the PTSM goal is decreased by an order of magnitude with the SVE enhancement of soil fracturing.

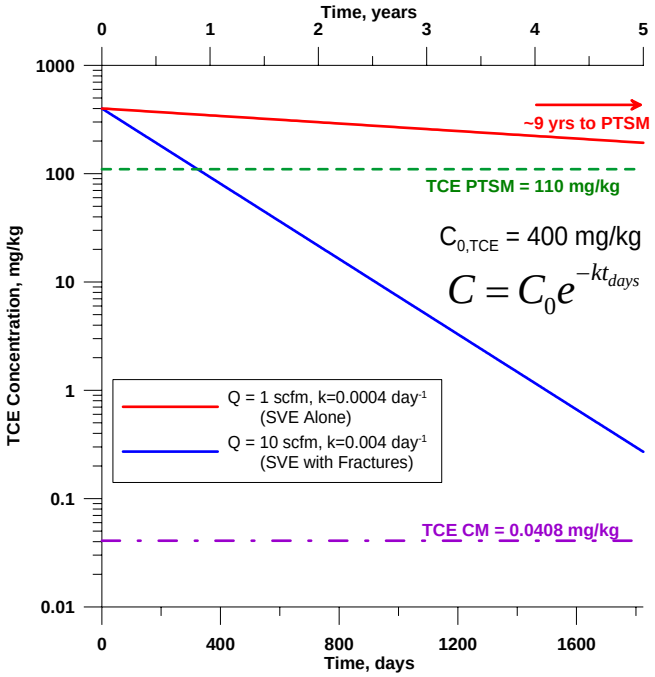

Figure 21 – Comparison of Soil Concentration Decline for TCE

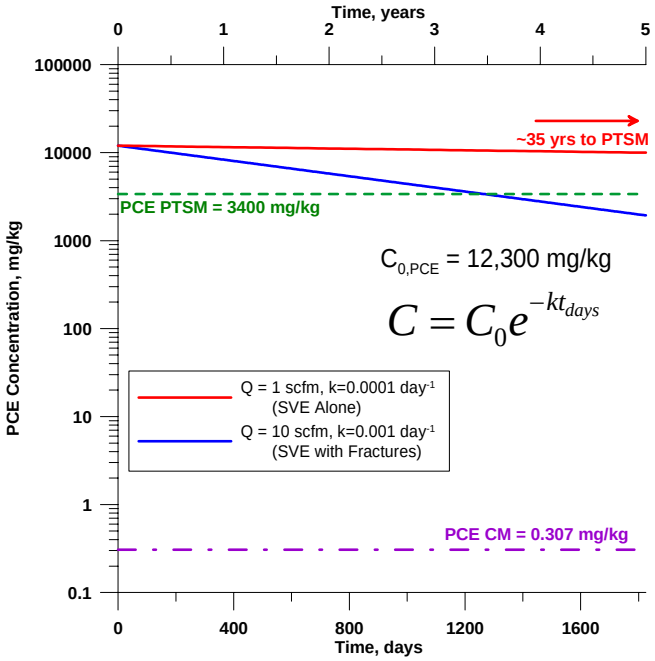

Figure 22 – Comparison of Concentration Decline for PCE

Extended SVE Testing

SVE was conducted for approximately 3 weeks on the extraction well (FRC-1E) and the largest fracture well (FRC-3F). The average flow rate was approximately 30 scfm at a system vacuum of 18 inches Hg. The daily removal rate was approximately 15 lbs/day TCE with a total of 217 lbs TCE removed during this testing period. Vapor concentrations declined from about 1500 ppmv to 900 ppmv TCE. This data is shown graphically in Figure 23. The increase in concentration on 9/23/05 occurred after pumping out water from the 5 ft long sump in the 4 inch extraction well. The water was approximately 1 ft into the screen zone.

During this short testing period, the concentration decay constant (*k*) was an order of magnitude higher than that estimated in the previous section. This increase may be due to a greater enhancement of SVE with fracturing than postulated based on flow rate alone, but a longer period of testing would be required to validate the continued trend.

Introducing sand-filled fractures into these tight zones improves the performance of SVE by 1) increasing the overall permeability of the formation and thereby increasing SVE flow rates, 2) shortening diffusion pathways, and 3) increasing air permeability by improving pore water removal. The synergistic effect of the fracture well completion methods, fracture and flow geometry, and pore water removal appears to increase the rate of solvent mass removal over that of increasing flow rate alone.

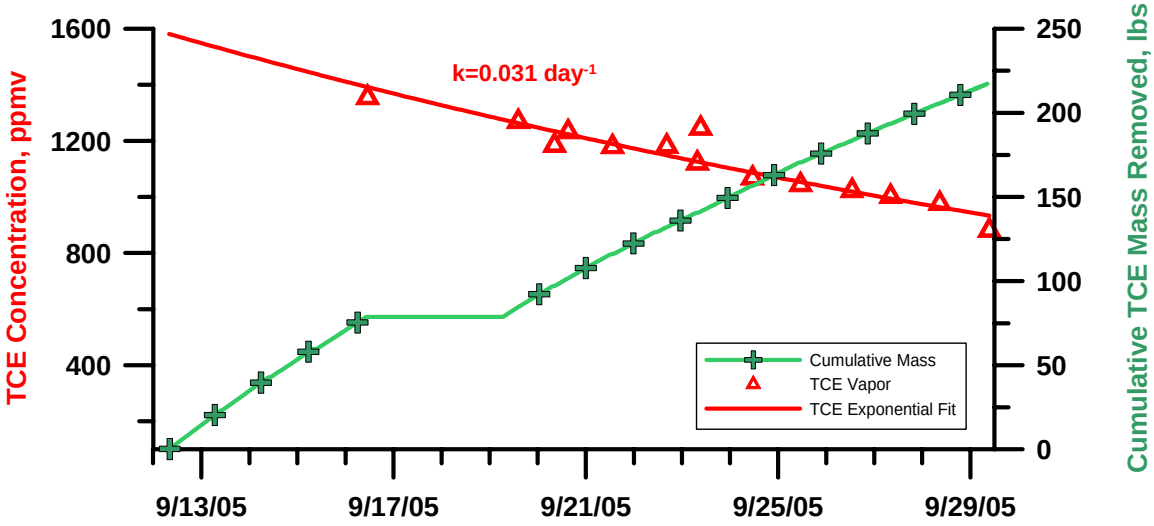

Figure 23 –Concentration and Mass Removal during Extended SVE Testing

The ZOI continually increased during the extended SVE testing as demonstrated by the continually increasing vacuum at the pressure monitoring points. This data is provided graphically in Figure 24 and shows the total flow rate from wells FRC-1E and FRC-3F, the total system vacuum and drawdown from selected

pressure monitoring points. Zero readings of the data result from shutting the system down to drain the water knockout tanks. Only lower reading vacuum ports could be measured due to over-ranging of the pressure transducers as indicated by the flat line from the 25 ft port. This increase in vacuum and ZOI is due to formation water drainage and the subsequent increased effective air permeability. Additional vacuum measurements from ports that exceeded the data logging transducers are provided in Table 10 and contours of the steady-state ZOI are provided in Figure 25. Using the fracture well FRC-3F in conjunction with the standard extraction well significantly increases the zone of influence. See Figure 17 and Figure 18 for comparison. The water removal is discussed in more detail in the following section.

Table 10 – Steady State Vacuum Readings on 9/16/05 (Flow=28.7 scfm)

Measurement Point	Vacuum Reading inches of water	Description
FRC-1E	243.0	4 inch extraction well
FRC-1F	37.0	22 ft fracture
FRC-2F	51.2	25 ft fracture
FRC-3F	224.0	28 ft fracture extraction well
FRC-1P 30 ft	88.5	5 ft from FRC-1E
FRC-2P 30 ft	81.5	10 ft from FRC-1E
FRC-4P 30 ft	141.1	8.7 ft from FRC-1E
SVE unit	266.0	total system vacuum

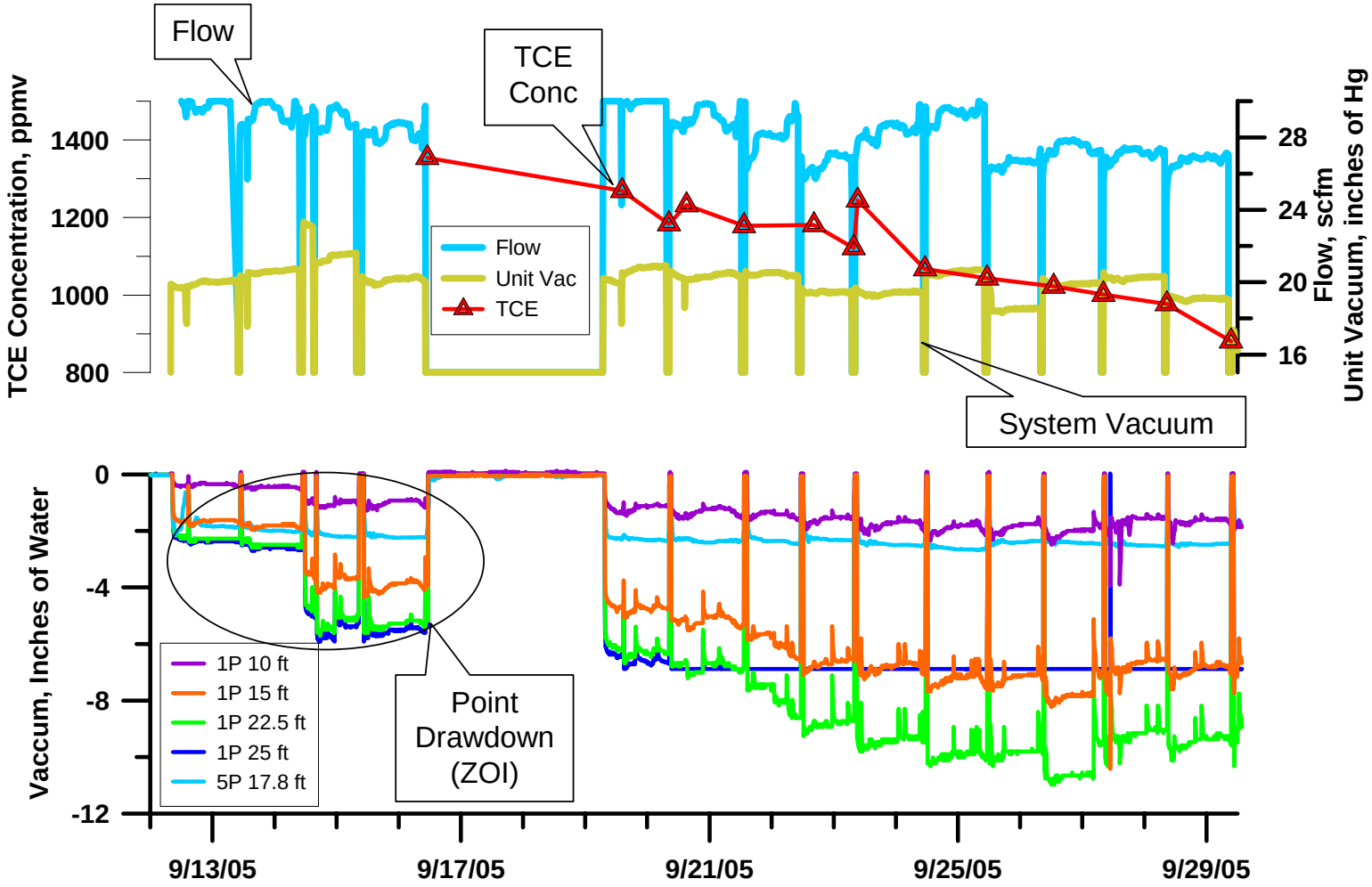

Figure 24 – Flow, System Vacuum and ZOI Pressure Measurements

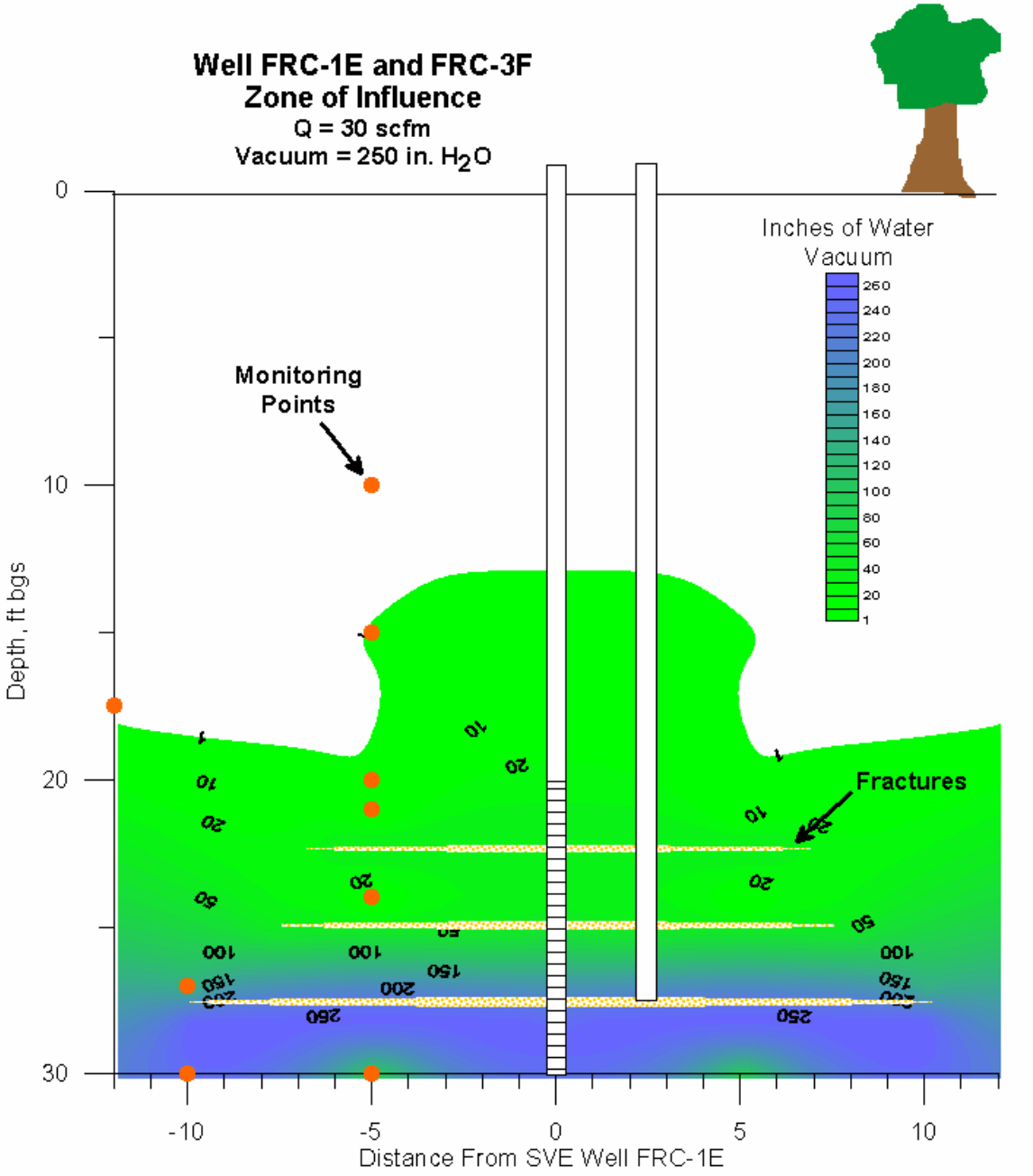

Figure 25 – Post-Fracture ZOI Contour for Pumping FRC-1E and Fracture FRC-3F Simultaneously

Interpretation of Pilot-Scale Results

It is possible to extrapolate the results of the short test to longer time by assuming the exponential decrease in concentrations is maintained. Integrating the mass rate of recovery and assuming an exponential decrease in concentration gives the total mass recovered from the well as

$$M_{total} = \frac{C_o Q M_w P_{atm}}{RTk}$$

where C_o is the initial concentration in the gas (ppmv), Q is the volumetric air recovery rate at standard state, M_w is the molecular weight of TCE, P_{atm} is atmospheric pressure, R is the gas constant, and k is the concentration decay constant (0.031 day^{-1} in this case).

This gives an estimate of the total mass of contaminants that could be recovered from the fractured well as 318 kg (700 lbs mass), which is roughly 3 times the mass recovered during the pilot operation. The rate of recovery will diminish with time. Most (99%) of the maximum recoverable mass will be removed in 150 days, based on the assumptions outlined above.

The area affected by this process can be estimated by recognizing the average concentration of TCE in the soil in the vicinity of the pilot site is 80 mg/kg (from Figure 12). This implies that the total TCE that could be recovered (318 kg) would be distributed within $2x10^3$ m^3 of contaminated soil. The contaminated region is assumed to be 3 m thick (Figure 12 and Figure 13). This gives 15 m as the estimated radial distance remediated by the well.

The distance could be considerably less than 15 m, if the well was recovering contaminants from zones of high concentration that were not discovered during the characterization effort. The affected area could be greater than 15 m, however, if the contaminants were completely removed near the well and only partially removed from the more distant regions. A variety of other factors could also contribute to uncertainty, so the estimate of 15m should be viewed as preliminary.

Evaluation of Water Generation

A significant amount of water was produced during the SVE testing and a continuous stream of water was observed in the hose from the fracture well FRC-3F. The vapor flow rate from the fracture was high enough so that water droplets were transported to the surface via the effluent gas stream from a depth of 28 ft. This data is plotted in Figure 26 and shows the daily volume of water removed, the cumulative water removed and the SVE system flow rate. Approximately 550 gallons of water were injected during fracturing and were removed prior to the data shown in this plot. The water removal was fairly constant during this short test period and averaged 66 gallons per day. Over a longer operating period, the amount of water generated will decrease with time as the pore water is drained.

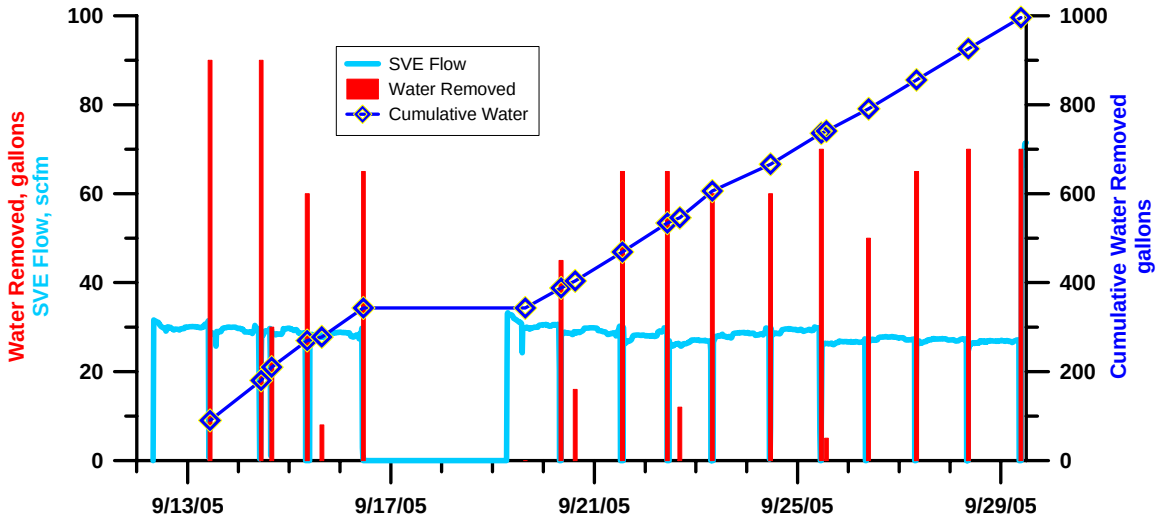

Figure 26 – Water Generation during SVE on FRC-1E and FRC-3F

The water in the vadose zone is from water injected during the hydraulic fracturing, natural capillary pore water, and rainfall infiltration. The volume of water injected with guar/sand slurry is known. The amount of water from capillary moisture and rainfall can be estimated. The fracture can be idealized as a flat, circular, high permeability zone at the bottom of a soil column. For simplicity, a 10 ft radius by 10 ft high soil cylinder is used for calculation purposes and is conceptually illustrated in Figure 27. The water loading into the fracture from rainfall infiltration is straight forward. With the 15 inches per year of rainfall infiltration used at the SRS, 8 gallons a day on average will load into the fracture from the 10 ft radius soil column.

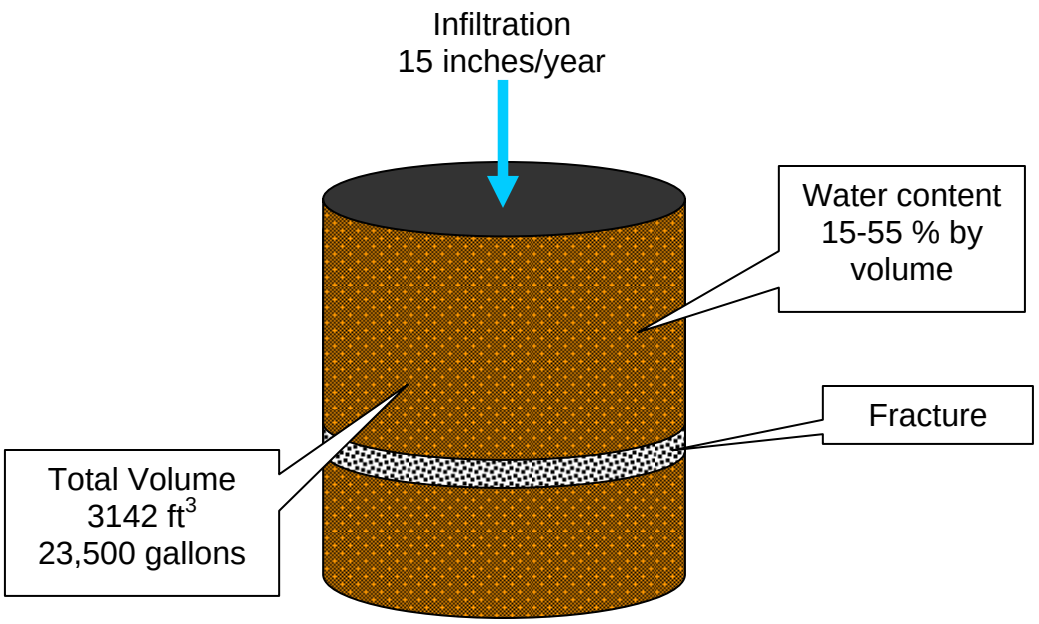

Figure 27 – Soil Column Conceptual Model for Water Generation

Placing a vacuum on the fracture is a similar concept as the laboratory pressure plate test used to measure soil capillary moisture relationships. This test determines the equilibrium soil moisture content retained in a soil subjected to a given soil-water tension (pressure). Another name for the results of this test is the soil water drainage curve. Placing a high vacuum on the fracture will initiate drainage of the soil column above and below the fracture.

Drainage curves from four samples in the Upland Unit are provided in Figure 28. These were plotted on a log pressure scale and show the water (percent by soil volume) that can be drained at a given pressure. The yellow shaded region is the range of vacuum applied during SVE on the fracture Well FRC-3F and the red line is the maximum achievable vacuum (1 atm). Based on these drainage curves, 5-15% of the pore water can by removed during SVE at these vacuums. Using the volume of the 10 ft radius by 10 ft high cylinder, 1,200 to 3,500 gallons of pore water could be drained into the fracture during SVE.

Since SVE relies on subsurface air flow to remove the volatile solvents, this water needs to be removed from the fracture for efficient remediation. Dual phase removal can be used to remove vapors and water at the same time. An added benefit to this water removal is the increase in effective air permeability and ZOI. As this water is removed, air flow and ZOI will increase. SVE can be limited due to mass transfer resistance of the hydrophobic compounds by trapped interparticle water and diffusion resistance from this water. Therefore, the water removal provides the benefits of increasing air flow and ZOI and decreasing some of the mass transfer limitations. The horizontal geometry of the

fractures significantly aids this water removal compared to SVE using standard vertical wells.

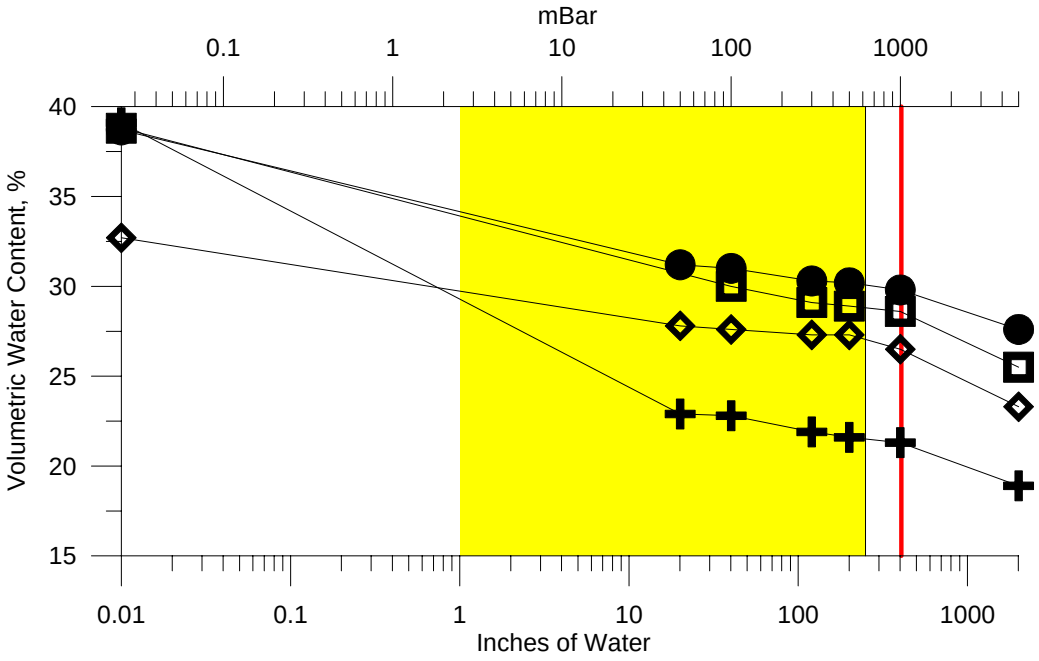

Figure 28 – Log Scale Water Drainage Curves from Soil Samples in the Upland Unit

Summary and Conclusions

Overall, SVE enhanced with soil fracturing appears valuable for accelerating solvent removal from the Upland Unit at the SRS. The following conclusions are drawn from this pilot testing:

- Fractures in the Upland Unit can increase flow rate and VOC mass removal by at least one order of magnitude over SVE alone.
- The Upland Unit is very conducive to fracturing.
- Fractures are fairly horizontal in virgin ground.
- Radii of 10 to 15 ft can be expected in the SRS Upland Unit
- Flow results show that fracturing to existing wells is not very effective.
- Using the fracture points as SVE wells will provide the most effective remediation.
- Numerical modeling shows the existence of a very low permeability 'well skin' around the conventionally installed SVE well.
- Installing wells to intersect the fractures after fracturing will only be effective if the well skin effects can be overcome. The feasibility of effectively doing this is unclear.
- For production work, fractures can be made through direct push rods and pre-packed wells can be installed.
- Pore water removal provides the added benefits of increasing air flow and ZOI and decreasing some mass transfer limitations.
- Introducing sand-filled fractures into these tight zones improves the performance of SVE by 1) increasing the overall permeability of the formation and thereby increasing SVE flow rates, 2) shortening diffusion pathways, and 3) increasing air permeability by improving pore water removal.
- The synergistic effect of the fracture well completion methods, fracture and flow geometry, and pore water removal appears to increase the rate of solvent mass removal over that of increasing flow rate alone.

Design Considerations for SVE with Fractures

The primary difference between a standard SVE remediation and SVE with fractures will be the amount of water generated due to the laterally extensive higher permeability zone. Rain infiltration and natural pore water removal will be a continuous source of water in the fractures that will need to be removed for optimal SVE performance. Dual phase systems to remove both gas and water have been demonstrated during this pilot study. Larger water knockout tanks will need to be designed with automated emptying for cost effective operations. In addition, the following can be considered for optimal and cost-effective remediation with fractures:

1. Install fractures in the tightest and highest concentration layers to take advantage of the horizontal geometry of the fractures
    a. Lateral fracture spacing should be on the order of 20 to 25 ft assuming a 10 ft fracture radius.
    b. Vertical fracture spacing should be as close as fiscally and physically possible and on the order of 3 to 5 ft. Higher vertical density of fractures will decrease the SVE remediation time.
2. Use portable SVE systems to increase flexibility in optimizing removal.
3. Install pressure and gas monitoring points to evaluate remediation effectiveness.
4. During startup testing, perform transient pumping tests to determine zone of influence (ZOI).
5. Design a monitoring program that includes periodic ZOI evaluations and depth discrete gas concentration measurements to aid in focusing the remediation on the most contaminated areas.
6. Monitor mass removal rates and estimate soil concentration decline based on exponential removal for transition to the next phase of remediation.

References

Bradner, G. C. and L. C. Murdoch. 2005. “Effects of skin and hydraulic fractures on SVE wells.” Journal of Contaminant Hydrology **77**: 271-297

Eddy, C. A., B. B. Looney, J. M. Dougherty, T. C. Hazen and D. S. Kaback. 1991. Characterization of the Geology, Geochemistry, Hydrology and Microbiology of the In-Situ Air Stripping Demonstration Site at the Savannah River Site (U). Westinghouse Savannah River Company. Aiken, South Carolina 29808. WSRC-RD-91-0021.

Fisher, U., C. Hinz, R. Schulin and F. Stauffer. 1998. "Assessment of nonequilibrium in gas-water mass transfer during advective gas-phase transport in soils." Journal of Contaminant Hydrology **33**: 133-148.

Oostrom, M., C. Hofstee, R. J. Lenhard and T. W. Wietsma. 2003. "Flow behavior and residual saturation formation of liquid carbon tetrachloride in unsaturated heterogeneous porous media." Journal of Contaminant Hydrology **64**: 93-112.

Smith, J. L., D. D. Reible, Y. S. Koo and E. P. S. Cheah. 1996. "Vacuum extraction of a nonaqueous phase residual in a heterogeneous vadose zone." Journal of Hazardous Materials **49**: 247-265.

USEPA. 1993. Hydraulic Fracturing Technology, Technology Evaluation Report. USEPA Risk Reduction Engineering Laboratory, Office of Research and Development. Cincinnati, OH. EPA/540/R-93/505.

Yang, Y. J., T. M. Gates and S. Edwards. 1999. "SVE Design: Mass Transfer Limitation due to Molecular Diffusion." Journal of Environmental Engineering **125**(9): 852-860.

Attachment 1 – Soil Sampling and Analysis Methods and Results

CPT Wireline

The United States Department of Energy (DOE) cone penetrometer test (CPT) truck was used with the CPT wireline sampling system. Applied Research Associates (ARA) developed the CPT wireline system with funding from the Department of Energy's National Energy Technology Laboratory (NETL). The wireline sampling tool uses 2.25-inch diameter rods with a removable dummy push tip and core barrel with a locking mechanism that fits inside the push rods. The wireline tool allows the recovery of multiple soil samples without removing and reinserting the push rod string, significantly reducing the amount of time required to collect sediment samples.

VOC Soil Sampling

After the core was brought to the surface, a 2 cubic centimeter (cc) soil plug sample was collected using a modified plastic syringe. The plug was immediately transferred to a 22 ml glass headspace vial with 5 ml of nano-pure water. The vial was then sealed with a crimped Teflon-lined septum top for head-space analysis. Duplicate samples were collected at each depth. The core barrels were steam cleaned between use to remove any residual volatile organic compounds (VOCs).

Soil Headspace Analysis for VOCs

The technique used to prepare and analyze soil samples for VOC analysis is a modified version of EPA Method 5021 which has been used successfully at the SRS since 1991. Each sample is weighed and then analyzed on the HP 5890 Series II or HP 6890 gas chromatograph (GC) using an automated head space sampler at 70 C for equivalent water concentrations. The GC is equipped with an electron capture and flame ionization detector connected in parallel. The column is a Supelco - VOCOL™ megabore borosilicate glass (60 m x 0.76 mm ID x 1.5 µm film thickness) specifically developed for volatile priority pollutants (EPA Methods 502, 602, and 8240). Mass soil concentrations (ppmm, mg/kg) are calculated based on an equal head space volume from 7.5 ml of water standards and nominal 7 ml of water/soil matrix, and are corrected for the mass difference between the soil and water. The gas chromatograph is calibrated using purchased certified mixtures in methanol that are diluted in deionized water to specific concentrations. Two reagent blanks of pure deionized water are included after the high concentration standards to ensure the transfer lines and column are being adequately flushed of residual solvents. The standard concentrations used for each head space sample run are: 3, 5, 10, 50, 100, 1,000, and 10,000 ppb (µg/l). A selected suite of compounds was chosen based on the primary contaminants expected at SRS. The samples were analyzed for 1,1-dichloroethylene (1,1-DCE), benzene, carbon tetrachloride (CCl_4), cis-1,2-dichloroethylene (cis-DCE), trichlorofluoromethane (Freon-11), chloroform, Freon-113, methylene chloride (MECL), perchloroethylene (PCE),

1,1,1-trichloroethane (TCA), trichloroethylene (TCE), trans-1,2-dichloroethylene (trans-DCE), and toluene. The minimum detection limit (MDL) and minimum quantitation limit (MQL) for soil analysis is provided in Table A-1.

The data reported from these analyses are considered screening level data. Although standard laboratory methods are followed, the laboratory is not certified by any federal or state agency for analyses required for specific permit analysis requirements. All reported data should be accompanied with this flag.

Table A-1 – Soil Analysis Detection Limits

Compound	MDL (mg/kg)	MQL (mg/kg)	MQL (ug/kg)
1,1 DCE	0.002	0.003	3
Benzene	0.04	0.13	131
CCl_4	0.0001	0.003	3
cis-DCE	0.04	0.12	124
Freon-11	0.0001	0.003	3
Chloroform	0.0007	0.003	3
Freon-113	0.0003	0.003	3
MECL	0.02	0.07	67
PCE	0.0001	0.003	3
TCA	0.0003	0.003	3
TCE	0.0004	0.003	3
Trans-DCE	0.02	0.05	49
Toluene	0.004	0.013	13
Vinyl Chloride	estimated		

Attachment 1 – Soil Concentration

Boring ID	Depth, ft	Type	1,1 DCE	cis-DCE	PCE	TCA	TCE	Trans-DCE	Vinyl Chloride
FRC-1E	6	Duplicate	nd	nd	0.011	0.034	0.646	nd	nd
FRC-1E	7	Sample	nd	nd	0.013	0.080	0.686	nd	nd
FRC-1E	7	Duplicate	nd	nd	0.010	0.042	0.511	nd	nd
FRC-1E	8	Sample	nd	nd	0.012	0.096	0.577	nd	nd
FRC-1E	8	Duplicate	nd	nd	0.013	0.096	0.606	nd	nd
FRC-1E	9	Sample	nd	nd	0.012	0.124	0.455	nd	nd
FRC-1E	9	Duplicate	nd	nd	0.010	0.100	0.395	nd	nd
FRC-1E	11	Sample	nd	nd	0.007	0.019	0.213	nd	nd
FRC-1E	11	Duplicate	nd	nd	0.008	0.024	0.317	nd	nd
FRC-1E	12	Sample	nd	nd	0.009	0.008	0.231	nd	nd
FRC-1E	12	Duplicate	nd	nd	0.009	0.009	0.332	nd	nd
FRC-1E	13	Duplicate	nd	nd	0.017	0.000	0.129	nd	nd
FRC-1E	14	Sample	nd	nd	0.015	0.001	0.075	nd	nd
FRC-1E	14	Duplicate	nd	nd	0.022	0.001	0.101	nd	nd
FRC-1E	15	Sample	nd	nd	0.052	0.000	0.163	nd	nd
FRC-1E	15	Duplicate	nd	nd	0.050	0.001	0.153	nd	nd
FRC-1E	16	Duplicate	nd	nd	0.066	0.000	0.165	nd	nd
FRC-1E	17	Sample	nd	nd	0.175	0.001	0.379	nd	nd
FRC-1E	17	Duplicate	nd	nd	0.177	0.001	0.385	nd	nd
FRC-1E	18	Sample	nd	nd	0.192	0.002	0.456	nd	nd
FRC-1E	18	Duplicate	nd	nd	0.168	0.002	0.455	nd	nd
FRC-1E	19	Sample	nd	nd	0.461	0.001	1.285	nd	nd
FRC-1E	19	Duplicate	nd	nd	0.697	0.003	1.781	nd	nd
FRC-1E	20	Duplicate	nd	nd	1.649	0.002	8.464	nd	nd
FRC-1E	21	Sample	nd	nd	1.517	0.006	34.316	nd	nd
FRC-1E	21	Duplicate	nd	nd	2.553	0.008	55.161	nd	nd
FRC-1E	22	Sample	nd	nd	2.476	0.010	81.663	nd	nd

Boring ID	Depth, ft	Type	1,1 DCE	cis-DCE	PCE	TCA	TCE	Trans-DCE	Vinyl Chloride
FRC-1E	22	Duplicate	nd	nd	2.779	0.011	92.770	nd	nd
FRC-1E	23	Sample	nd	nd	0.282	0.004	23.678	nd	nd
FRC-1E	23	Duplicate	nd	nd	0.479	0.005	33.163	nd	nd
FRC-1E	24	Sample	nd	nd	0.552	0.010	92.549	nd	nd
FRC-1E	24	Duplicate	nd	nd	0.487	0.009	78.030	nd	nd
FRC-1E	27	Sample	nd	nd	0.556	0.012	105.897	nd	nd
FRC-1E	28	Sample	nd	nd	0.575	0.012	135.943	nd	nd
FRC-1E	29	Sample	nd	nd	0.582	0.011	146.937	nd	nd
FRC-1E	29	Duplicate	nd	nd	0.683	0.010	140.977	nd	nd
FRC-1E	30	Duplicate	nd	nd	0.120	0.007	69.182	nd	nd
FRC-1E	31	Sample	nd	nd	0.066	0.003	34.613	nd	nd
FRC-1E	31	Duplicate	nd	nd	0.085	0.005	46.355	nd	nd
FRC-1E	32	Sample	nd	nd	0.163	0.008	81.615	nd	nd
FRC-1E	32	Duplicate	nd	nd	0.142	0.008	74.354	nd	nd
FRC-1P	10	Sample	nd	nd	0.015	0.019	0.569	nd	nd
FRC-1P	10	Duplicate	0.007	nd	0.008	0.023	0.776	nd	nd
FRC-1P	11	Sample	nd	nd	0.010	0.005	0.266	nd	nd
FRC-1P	11	Duplicate	0.005	nd	0.009	0.007	0.589	nd	nd
FRC-1P	12	Sample	nd	nd	0.009	0.001	0.173	nd	nd
FRC-1P	12	Duplicate	0.003	nd	0.013	0.001	0.412	nd	nd
FRC-1P	13	Sample	nd	nd	0.011	0.000	0.112	nd	nd
FRC-1P	13	Duplicate	0.003	nd	0.011	0.001	0.115	nd	nd
FRC-1P	14	Sample	nd	nd	0.026	0.000	0.070	nd	nd
FRC-1P	14	Duplicate	0.003	nd	0.038	0.001	0.089	nd	nd
FRC-1P	15	Duplicate	0.002	nd	0.098	0.001	0.107	nd	nd
FRC-1P	16	Sample	nd	nd	0.212	nd	0.385	nd	nd
FRC-1P	16	Duplicate	0.008	nd	0.135	0.001	0.275	nd	nd
FRC-1P	17	Sample	0.002	nd	0.719	0.005	2.048	nd	nd
FRC-1P	17	Duplicate	0.004	nd	0.426	0.001	1.916	nd	nd

Boring ID	Depth, ft	Type	1,1 DCE	cis-DCE	PCE	TCA	TCE	Trans-DCE	Vinyl Chloride
FRC-1P	18	Sample	nd	nd	0.978	0.002	4.526	nd	nd
FRC-1P	18	Duplicate	0.002	nd	0.983	0.002	4.502	nd	nd
FRC-1P	19	Sample	nd	nd	0.441	0.002	4.882	nd	nd
FRC-1P	19	Duplicate	0.005	nd	0.484	0.001	4.283	nd	nd
FRC-1P	20	Sample	nd	nd	0.439	0.003	8.210	nd	nd
FRC-1P	20	Duplicate	0.002	nd	0.291	0.001	5.335	nd	nd
FRC-1P	21	Duplicate	0.005	nd	0.378	0.003	10.038	nd	nd
FRC-1P	22	Sample	nd	nd	0.372	0.005	17.047	nd	nd
FRC-1P	22	Duplicate	0.002	nd	0.368	0.005	19.751	nd	nd
FRC-1P	23	Sample	nd	nd	0.082	0.004	10.087	nd	nd
FRC-1P	23	Duplicate	0.006	nd	0.141	0.005	19.093	nd	nd
FRC-1P	24	Sample	nd	nd	0.059	0.004	9.382	nd	nd
FRC-1P	24	Duplicate	0.002	nd	0.253	0.007	25.388	nd	nd
FRC-1P	25	Duplicate	0.002	nd	0.247	0.006	25.183	nd	nd
FRC-1P	26	Sample	nd	nd	0.524	0.008	42.202	nd	nd
FRC-1P	26	Duplicate	0.003	nd	0.377	0.007	39.922	nd	nd
FRC-1P	27	Sample	nd	nd	0.236	0.005	31.334	nd	nd
FRC-1P	27	Duplicate	0.004	nd	0.446	0.006	44.542	nd	nd
FRC-1P	28	Sample	nd	nd	0.343	0.005	37.109	nd	nd
FRC-1P	28	Duplicate	0.006	nd	0.320	0.003	29.703	nd	nd
FRC-1P	29	Duplicate	0.005	nd	0.193	0.004	32.267	nd	nd
FRC-1P	30	Sample	nd	nd	0.040	0.004	15.089	nd	nd
FRC-1P	30	Duplicate	0.002	nd	0.047	0.003	16.131	nd	nd
FRC-2P	18	Sample	nd	nd	1.261	0.014	2.938	nd	nd
FRC-2P	18	Duplicate	0.003	nd	0.874	0.001	1.787	nd	nd
FRC-2P	19	Sample	nd	nd	2.498	0.012	7.893	nd	nd
FRC-2P	19	Duplicate	0.003	nd	2.461	0.002	6.963	nd	nd
FRC-2P	20	Sample	nd	nd	1.344	0.014	5.746	nd	nd
FRC-2P	20	Duplicate	0.008	nd	1.667	0.002	7.614	nd	nd

Boring ID	Depth, ft	Type	1,1 DCE	cis-DCE	PCE	TCA	TCE	Trans-DCE	Vinyl Chloride
FRC-2P	21	Sample	nd	nd	2.676	0.005	17.866	nd	nd
FRC-2P	21	Duplicate	0.004	nd	3.559	0.005	29.782	nd	nd
FRC-2P	22	Sample	nd	nd	0.047	nd	2.197	nd	nd
FRC-2P	22	Duplicate	0.004	nd	0.170	0.001	6.637	nd	nd
FRC-2P	23	Sample	nd	nd	1.249	0.009	79.247	nd	nd
FRC-2P	23	Duplicate	0.005	nd	0.632	0.004	39.306	nd	nd
FRC-2P	24	Sample	nd	nd	0.490	0.009	41.108	nd	nd
FRC-2P	24	Duplicate	0.005	nd	0.606	0.004	45.922	nd	nd
FRC-2P	25	Sample	nd	nd	0.907	0.007	70.822	nd	nd
FRC-2P	25	Duplicate	0.005	nd	0.877	0.007	73.086	nd	nd
FRC-2P	26	Sample	nd	nd	1.160	0.009	103.026	nd	nd
FRC-2P	26	Duplicate	0.007	nd	1.268	0.009	103.336	nd	nd
FRC-2P	27	Sample	nd	nd	1.251	0.010	124.860	nd	nd
FRC-2P	27	Duplicate	0.009	nd	1.476	0.011	142.390	nd	nd
FRC-2P	28	Sample	nd	nd	1.119	0.009	129.872	nd	nd
FRC-2P	28	Duplicate	0.008	nd	1.192	0.008	128.923	nd	nd
FRC-2P	29	Sample	nd	nd	1.069	0.008	133.819	nd	nd
FRC-2P	29	Duplicate	0.009	nd	1.303	0.008	148.334	nd	nd
FRC-2P	30	Sample	nd	nd	0.338	0.005	55.294	nd	nd
FRC-3P	13	Sample	nd	nd	0.081	0.000	0.505	nd	nd
FRC-3P	14	Sample	nd	nd	0.274	0.000	0.512	nd	nd
FRC-3P	15	Sample	nd	nd	0.372	0.000	0.153	nd	nd
FRC-3P	16	Sample	nd	nd	1.230	0.000	0.992	nd	nd
FRC-3P	17	Sample	nd	nd	0.897	0.000	0.218	nd	nd
FRC-3P	18	Sample	nd	nd	0.265	0.000	0.691	nd	nd
FRC-3P	19	Sample	nd	nd	0.742	0.001	3.128	nd	nd
FRC-3P	20	Sample	0.003	nd	1.383	0.002	14.978	nd	nd
FRC-3P	21	Sample	nd	nd	0.176	0.000	3.995	nd	nd
FRC-3P	22	Sample	nd	nd	0.099	0.000	3.656	nd	nd

Boring ID	Depth, ft	Type	1,1 DCE	cis-DCE	PCE	TCA	TCE	Trans-DCE	Vinyl Chloride
FRC-3P	23	Sample	nd	nd	0.154	0.000	6.260	nd	0.039
FRC-3P	24	Sample	nd	nd	0.131	0.000	5.652	nd	nd
FRC-3P	25	Sample	0.004	nd	0.362	0.001	13.788	nd	nd
FRC-3P	26	Sample	0.004	nd	0.984	0.004	48.674	nd	nd
FRC-3P	27	Sample	0.005	nd	1.249	0.009	81.158	nd	nd
FRC-3P	28	Sample	0.005	nd	1.315	0.009	91.843	nd	nd
FRC-3P	29	Sample	0.004	nd	0.748	0.004	53.797	nd	0.021
FRC-3P	30	Sample	0.001	nd	0.560	0.003	45.905	nd	nd
FRC-4P	13	Sample	nd	nd	0.004	0.000	0.268	nd	nd
FRC-4P	14	Sample	nd	nd	0.007	nd	0.267	nd	nd
FRC-4P	15	Sample	nd	nd	0.007	nd	0.135	nd	nd
FRC-4P	16	Sample	nd	nd	0.007	nd	0.066	nd	nd
FRC-4P	17	Sample	nd	nd	0.006	nd	0.060	nd	nd
FRC-4P	18	Sample	nd	nd	0.026	0.000	0.178	nd	nd
FRC-4P	19	Sample	nd	nd	0.028	0.000	0.258	nd	nd
FRC-4P	20	Sample	nd	nd	0.032	0.000	0.558	nd	nd
FRC-4P	21	Sample	nd	nd	0.010	nd	0.375	nd	0.035
FRC-4P	22	Sample	nd	nd	0.034	0.000	1.230	nd	nd
FRC-4P	23	Sample	nd	nd	0.013	nd	0.829	nd	nd
FRC-4P	24	Sample	0.008	nd	0.047	0.000	2.148	nd	0.067
FRC-4P	25	Sample	0.003	nd	0.232	0.002	8.398	nd	nd
FRC-4P	26	Sample	0.001	nd	0.286	0.002	11.495	nd	nd
FRC-4P	27	Sample	0.001	nd	0.224	0.002	9.195	nd	0.024
FRC-4P	28	Sample	0.010	nd	0.144	0.002	8.363	nd	0.047
FRC-4P	29	Sample	nd	nd	0.025	0.001	2.107	nd	nd
FRC-5P	20	Sample	nd	nd	0.002	nd	0.015	nd	0.005
FRC-5P	21	Sample	nd	nd	0.004	nd	0.078	nd	0.004
FRC-5P	22	Sample	nd	nd	0.004	0.000	0.085	nd	nd
FRC-5P	23	Sample	nd	nd	0.004	0.000	0.104	nd	nd

Boring ID	Depth, ft	Type	1,1 DCE	cis-DCE	PCE	TCA	TCE	Trans-DCE	Vinyl Chloride
FRC-5P	24	Sample	nd	nd	0.008	0.001	0.457	nd	nd
FRC-5P	25	Sample	nd	nd	0.014	0.001	1.045	nd	nd
FRC-5P	26	Sample	nd	nd	0.033	0.002	2.969	nd	nd
FRC-5P	27	Sample	nd	nd	0.030	0.002	3.007	nd	nd
FRC-5P	28	Sample	nd	nd	0.032	0.003	3.432	nd	nd
FRC-6P	20	Sample	nd	nd	0.001	nd	0.009	nd	nd
FRC-6P	21	Sample	nd	nd	0.001	nd	0.008	nd	nd
FRC-6P	22	Sample	nd	nd	0.001	nd	0.008	nd	nd
FRC-6P	23	Sample	nd	nd	0.002	nd	0.014	nd	nd
FRC-6P	24	Sample	nd	nd	0.004	0.000	0.043	nd	nd
FRC-6P	25	Sample	nd	nd	0.008	0.000	0.083	nd	nd
FRC-6P	26	Sample	nd	nd	0.008	0.000	0.144	nd	nd
FRC-6P	27	Sample	nd	nd	0.004	0.000	0.079	nd	nd
FRC-6P	28	Sample	nd	nd	0.010	0.001	0.290	nd	nd
FRC-6P	29	Sample	nd	nd	0.000	nd	0.001	nd	nd
FRC-7P	16	Sample	nd	nd	0.000	nd	0.001	nd	nd
FRC-7P	17	Sample	nd	nd	0.000	nd	0.001	nd	nd
FRC-7P	18	Sample	nd	nd	0.000	nd	0.004	nd	nd
FRC-7P	19	Sample	nd	nd	0.001	nd	0.006	nd	nd
FRC-7P	20	Sample	nd	nd	0.001	nd	0.009	nd	nd
FRC-7P	21	Sample	nd	nd	0.001	nd	0.012	nd	nd
FRC-7P	22	Sample	nd	nd	0.001	nd	0.011	nd	nd
FRC-7P	23	Sample	nd	nd	0.002	0.000	0.025	nd	nd
FRC-7P	24	Sample	nd	nd	0.002	nd	0.030	nd	nd
FRC-7P	25	Sample	nd	nd	0.008	0.000	0.141	nd	nd